Master Thesis

# Trajectory Optimization For High-Speed Flight Phases of Commercial Aircraft

Master of Science in Aerospace Engineering

*Author:*
López Platero, Alberto

*Supervisors:*
**[Capgemini]** Ahmed, Kawser
**[ISAE Supaero]** Pastor, Philippe

## Declaration of Authenticity

This assignment is entirely my own work. Quotations from literature are properly indicated with appropriated references in the text. All literature used in this piece of work is indicated in the bibliography placed at the end. I confirm that no sources have been used other than those stated.

I understand that plagiarism (copy without mentioning the reference) is a serious examinations offence that may result in disciplinary action being taken.

Date **10/10/2024** Signature

**Abstract**

The aviation industry faces increasing pressure to enhance operational efficiency due to rising fuel costs and growing environmental concerns. With air traffic projected to grow by 4.3 % annually over the next two decades, the contribution of aviation to global $CO_2$ emissions is expected to increase significantly. This study focuses on the development of an advanced trajectory optimization tool for commercial aircrafts to minimize the cost per flight and reduce the environmental impact. The Aircraft Trajectory Optimization Problem (TOP) is formulated as an Optimal Control Problem (OCP) and solved using direct numerical methods, which convert the problem into a Non-linear Programming (NLP) problem. A collocation based approach implemented in the DYmos tool is utilized, employing the Base of Aircraft Data (BADA) performance model. Surrogate modeling techniques are applied to build data-driven approaches from engine thrust, specific fuel consumption and atmospheric wind models. A special focus in the search for a proper initial approach and the automatic implementation is undertaken to increase the convergence. The results indicate significant potential for reducing fuel consumption and emissions through optimized flight trajectories.

**Keywords**: Multiphase trajectory optimization, optimal control, direct collocation, commercial aircraft, fuel consumption minimization, surrogate model, wind model

# Contents


**1 Introduction** **7**
1.1 Objectives . . . 8
1.2 Outline of the Thesis . . . 8

**2 State of the Art** **10**
2.1 Definition of an Optimal Control Problem . . . 10
2.2 Numerical Approaches . . . 11
2.2.1 Indirect methods . . . 11
2.2.2 Direct methods . . . 11
2.3 Solutions Approaches . . . 12
2.4 Exploring Surrogate Model Techniques . . . 12
2.5 Exploring Initial Guess Determination Techniques . . . 13

**3 Workspace** **14**

**4 Methodology** **15**
4.1 Aircraft Flight Dynamics . . . 15
4.1.1 Reference System . . . 15
4.1.1.1 Earth Axes System . . . 15
4.1.1.2 Geographic Axes System . . . 15
4.1.1.3 Local Horizon Axes System . . . 16
4.1.1.4 Wind Axes System . . . 17
4.1.1.5 Body Axes System . . . 18
4.1.2 Equations of motion . . . 20
4.1.2.1 Kinematic equations . . . 21
4.1.2.2 Dynamic equations . . . 22
4.2 Performance Model . . . 25
4.2.1 BADA user manual . . . 25
4.2.1.1 Standard Atmosphere . . . 25
4.2.1.2 Aerodynamics . . . 26
4.2.1.3 Engine Thrust . . . 27
4.2.1.4 Fuel Consumption . . . 28
4.2.2 Surrogate model . . . 28
4.2.2.1 Kringing method . . . 29
4.2.2.2 Neural Networks . . . 29
4.2.3 Introduction of wind effects . . . 31
4.3 Formulation of Aircraft Trajectory Optimization Problem . . . 33
4.3.1 Problem definition . . . 33
4.3.2 Optimal control transcriptions . . . 36
4.3.3 Collocation . . . 37
4.3.4 Determination of initial guess . . . 37

**5 Results** **40**
5.1 Case Study 1: Analysis of Surrogate Model Performance . . . 40
5.2 Case Study 2: Cost Index Influence. Pareto Front . . . 42
5.3 Case Study 3: Analysis of Wind Effects in Route Optimization . . . 44

**6 Conclusions** **47**

**7 Future Work** **49**

# Nomenclature

| Symbols | Definition | Magnitude |
|---|---|---|
| $\alpha$ | angle of attack | rad |
| $\beta$ | side slip angle | rad |
| $\gamma$ | flight path angle | rad |
| $\chi$ | yaw angle of velocity | rad |
| $\delta$ | change in value | - |
| $\epsilon$ | thrust angle of attack | rad |
| $\epsilon_0$ | nominal direction between axial's aircraft body frame and engine | rad |
| $\lambda$ | latitude | rad |
| $\mu$ | roll angle of velocity | rad |
| $\nu$ | thrust side slip angle | rad |
| $\omega$ | angular velocity | rad/s |
| $\phi$ | roll angle | rad |
| $\psi$ | heading angle | rad |
| $\rho$ | air density | $kg/cm^3$ |
| $\tau$ | air temperature | $K$ |
| $\theta$ | longitude | rad |
| $a$ | speed of sound | $m/s$ |
| $C$ | total cost | € |
| $C_C$ | fixed costs | € |
| $C_D$ | drag coefficient | - |
| $C_{D0}$ | parasitic drag coefficient | - |
| $C_{D2}$ | induced drag coefficient | - |
| $C_F$ | cost of fuel per kilogram | €$/kg$ |
| $C_L$ | lift coefficient | - |
| $C_T$ | cost of time per minute of flight | €$/min$ |
| $C_{Tc1}$ | 1st maximum climb thrust coefficient | $N$ |
| $C_{Tc2}$ | 2nd maximum climb thrust coefficient | $feet$ |
| $C_{Tc3}$ | 3rd maximum climb thrust coefficient | $1/feet^2$ |
| $C_{Tc4}$ | 1st thrust temperature coefficient | $deg.C$ |
| $C_{Tc5}$ | 2nd thrust temperature coefficient | $1/deg.C$ |
| $C_{Tcr}$ | maximum cruise thrust coefficient | - |
| $C_{Tdes}$ | descent thrust coefficient | - |
| $C_{f1}$ | 1st thrust specific fuel consumption coefficient | $kg/min/kN$ |
| $C_{f2}$ | 2nd thrust specific fuel consumption coefficient | $knots$ |
| $C_{f3}$ | 1st descent fuel flow coefficient | $kg/min$ |
| $C_{f4}$ | 2nd descent fuel flow coefficient | $feet$ |
| $C_{fr}$ | cruise fuel flow correction coefficient | - |
| $CI$ | cost index | - |
| $D$ | axial drag force | $N$ |
| $\Delta F$ | trip fuel | $kg$ |
| $\Delta T$ | flight duration | $min$ |
| $F$ | force | $N$ |
| $g$ | gravity force | $N$ |
| $h$ | altitude | $m$ |
| $J$ | objective function | - |
| $L$ | lift force | $N$ |

| Symbols | Definition | Magnitude |
|---|---|---|
| $m$ | mass | $kg$ |
| $MTOW$ | Maximum Take Off Weight | - |
| $OEW$ | Operational Empty Weight | - |
| $p$ | pressure | $Pa$ |
| $Q$ | side force | $N$ |
| $R_T$ | Earth radius | $m$ |
| $S$ | surface | $m^2$ |
| $T$ | thrust | $N$ |
| $Tr$ | transformation matrix | - |
| $\overline{d}$ | parameters vector | - |
| $\overline{g}_0$ | initial boundary constraint | - |
| $\overline{g}_f$ | final boundary constraint | - |
| $\overline{p}$ | path constraint | - |
| $\overline{u}$ | dynamic control variables vector | - |
| $\overline{x}$ | state variables vector | - |
| $\vec{i}$ | unit vector of x axis | - |
| $\vec{j}$ | unit vector of y axis | - |
| $\vec{k}$ | unit vector of z axis | - |
| $\vec{r}$ | position vector | $m$ |

| Subscripts | Definition |
|---|---|
| $lb$ | lower bound |
| $ub$ | upper bound |
| $E$ | Earth axes system |
| $G$ | geographic axes system |
| $h$ | local horizon axes system |
| $w$ | wind axes system |
| $b$ | body axes system |
| $I$ | inertial |
| $A$ | aerodynamic |
| $T$ | thrust |
| $trop$ | tropopause |
| $ISA$ | International Standard Atmosphere |
| 0 | initial |
| $f$ | final |
| $CL$ | climb |
| $CR$ | cruise |
| $DES$ | descent |

| Suprascript | Definition |
|---|---|
| $GE$ | from geographical to Earth axes system |
| $GX$ | from geographical to auxiliary I axes system |
| $XE$ | from auxiliary I to Earth axes system |
| $G$ | geographic axes system |

# 1 Introduction

Humankind has been undoubtedly influenced by technology and engineering milestones throughout history. This tendency has enabled humanity to thrive from the discovery of fire and the mastery of metallurgy, in the early stages of history, towards the arrival of the Internet era and the conquer of the space and skies. Words such as *progress* or *evolution* come along when reminiscing our past, but also when projecting onto the future. Our never-ending willingness to prosper has inexorably led us to a search for ingenious solutions that ensure our evolution, solutions which have gradually become more effective, and thus finding a focal point in the optimization of processes.

Optimization is a discipline of paramount importance in every domain, yielding a performance enhancement linked to cost reduction, resource efficiency and more sustainable solutions. Following this principle, aerospace engineering have rocketed astonishingly the last 70 years making it accessible and crucial to many people, thanks to the last advancements in which the search for optimal solutions has been the main goal to pursue. More efficient engines, lighter structures and more aerodynamic shapes have enabled the miracle of connecting distant nodes of the globe at a lower price and time. In the last years, governments have set targets to build a path towards industry decarbonization emphasizing efficiency and sustainability. Within this context, developing tools to optimize commercial aircraft trajectories has become a critical focus.

Although the aerospace industry seems to be reaching a technological asymptote of improvement, infinitesimal margins of change still entail significant profits. Hence optimization problems need to account for larger amounts of constraints and variables in order to ensure minimal upgrades. It is within this context that this study is born.

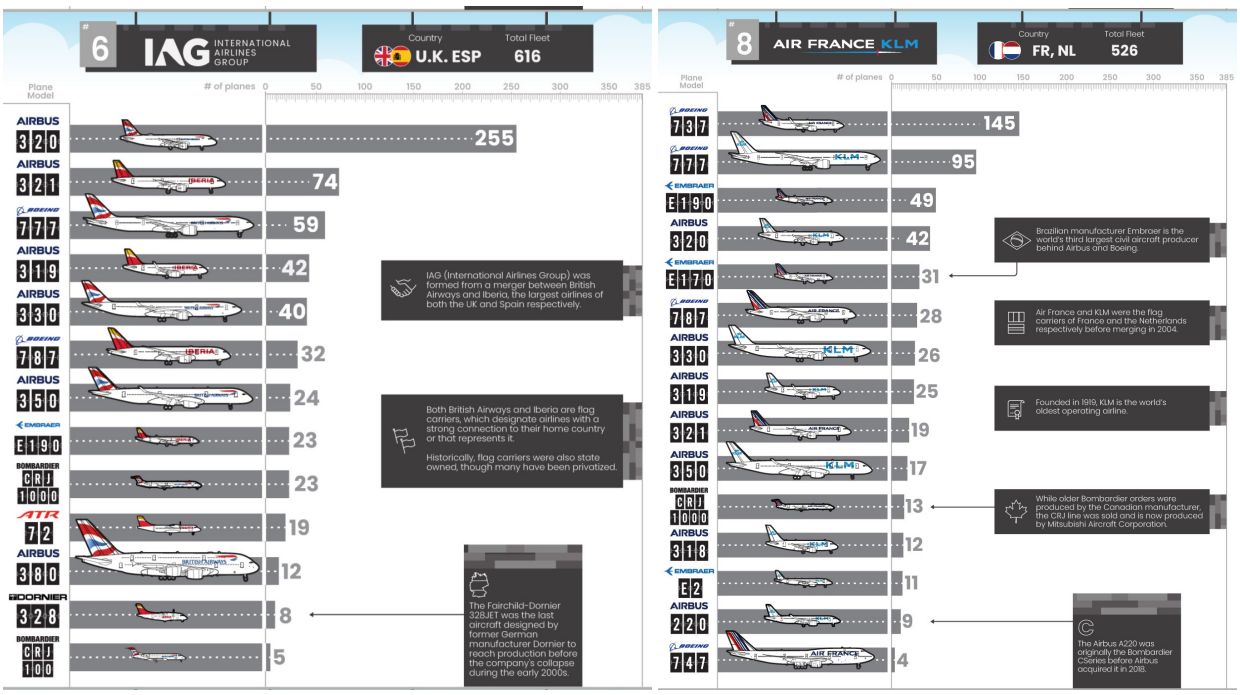


(a) International Airlines Group fleet

(b) Air France-KLM fleet

Figure 1.1: Fleet of the two biggest European airlines [8]

Trajectory optimization is the process of determining the most efficient path while meeting specific performance criteria and constraints. In the competitive sector of airlines, time, fuel cost and punctuality are critical parameters to set a difference with the competitors and be able to have a greater margin. In order to understand how important is to reduce the costs, a 1% of fuel saving in a flight from Madrid to London means that approximately 60 kilograms of fuel are saved (in the case of a medium sized plane, A320). In the actual market

(September 2024), the value of this fuel saved is 48€. If the average number of flights per day for a plane is 5 and a medium-size fleet airline can reach up to 100 aircrafts (for a specific model). This 1% fuel saving will yield an annual saving of 8 760 000€. In fact, some big European airlines such as AirFrance-KLM group or IAG group, as shown in figure 1.1, deal with bigger fleets, so the profit margin could be even bigger.

Given the potential of a mere 1% improvement, it is crucial to research and develop solvers able to replicate more realistic and accurate solutions in order to move aviation towards a more sustainable and green future. The goal of the following study is to set the objective and methodology of the upcoming optimization tool. Features as the determination of the initial guess, the development of surrogate models and the introduction of atmospheric conditions are key challenges studied to design more refined and competitive solutions.

## 1.1 Objectives

This thesis will delve into the complex problem of trajectory optimization and will tackle the main difficulties that optimization problems present, such as convergence, robustness or computational time while maintaining a sufficiently accurate solution. The complexity of this optimization task arises from the need to consider multiple factors simultaneously and a big amount of segments to properly control the trajectory.

Achieving an optimal solution within a reasonable time frame poses significant challenges, particularly in terms of computational efficiency and convergence. Optimization solvers highly rely on the selection of a suitable initial guess whose closeness to the optimal solution will determine, to a large extent, the performance of the tool.

The objectives of this study are:

- **O.1 Develop a robust trajectory optimization tool** for commercial aircrafts capable to determine the most cost-effective flight route between two airports.
- **O.2 Generate an automatic initial guess** to conceive a more user-friendly tool. Thus, the inputs introduced by the user are focused on the configuration of the route settings such as the departure and arrival airport features.
- **O.3 Develop strategies for generating accurate initial guesses** improving the likelihood of convergence to a global optimum while reducing the time and computational resources.
- **O.4 Ensure the versatility of the tool** aiming to be able to run any case in the whole globe and guarantee the robustness of the optimization.
- **O.5 Generate valid surrogate models** to substitute the analytical models. The objective is to create data-driven models and be able to reproduce a more realistic scenarios. The key challenge is to reach high accuracies and a proper generalization of the data.

## 1.2 Outline of the Thesis

1. **Introduction.** This chapter outlines the aviation industry's push toward a more sustainable future and emphasizes the importance of developing new tools to ensure fuel efficiency. The research problem is framed, and the objectives of the thesis are clearly introduced.
2. **State of the Art.** A comprehensive review of the existing literature is presented, starting with a formal definition of an Optimal Control Problem. This is followed by an in-depth analysis of available numerical methods, including indirect and direct approaches, as well as various solution strategies. Additionally, surrogate modeling techniques and methods for determining initial guesses are explored.
3. **Workspace.** This chapter introduces the company in which this research was conducted and highlights the role of the department responsible for the conception of the tool. The environment in which the tool was developed is described in detail.

4. **Methodology.** The problem-solving approach is presented, focusing on key aspects of aircraft flight dynamics control. This includes the equations of motion, the performance model, initial guess determination, and the methodology employed to solve the dynamic optimization problem. The chapter also explains how wind effects are incorporated into the model.

5. **Results.** Three case studies are conducted to assess the tool's performance across five objectives established earlier in the thesis. These cases include evaluating the surrogate model's effectiveness, the influence of cost index on optimization, and the impact of wind conditions on route optimization.

6. **Conclusions.** This chapter summarizes the research findings, highlighting the key contributions and insights gained. An evaluation of how well the initial objectives were achieved is also provided.

7. **Future Work.** The thesis concludes with recommendations for future research, outlining potential improvements and extensions to the work based on the results and limitations encountered during the study.

# 2 State of the Art

Optimizing commercial aircraft performance is a complex task that involves numerous variables and constraints. To effectively address this challenge, researchers and engineers employ a variety of advanced techniques and methodologies.

## 2.1 Definition of an Optimal Control Problem

Optimal control implies the optimization of a dynamical system. Typically this takes the form of a trajectory in which the states of the system evolve with time. The evolution of the states ($\overline{x}$) are typically governed by an ordinary differential equation (ODE). Thus, the dynamics are characterized as,

$$\dot{\overline{x}} = f_{ode}\left(\overline{x}, t, \overline{u}, \overline{d}\right) \tag{2.1}$$

where $\overline{x}$ are the state variables, $t$ the time, $\overline{u}$ the dynamic control variables and $\overline{d}$ the parameters.

When optimizing problems there will be constraints on the system. There are several types of constraints, firstly, constraints can be characterized by bounding the initial states and time of a trajectory. Thus, $\overline{x}$, $t$, $\overline{u}$ and $\overline{d}$ can be set with lower and upper bounds along the trajectory.

As well, non-linear constraints can be added to the optimization problem. They are useful to bound an output of the system at a specific point along the trajectory (boundary constraints, $\overline{g}$) or along the entire trajectory (path constraints, $\overline{p}$).

Additionally, the optimization problem is designed to minimize or maximize an objective function, which can be defined as,

$$J = f_{ode}\left(\overline{x}, t, \overline{u}, \overline{d}\right) \tag{2.2}$$

Typically, this objective function will represent the fuel consumption, the time or the cost per flight.

Finally, the overall optimization problem structure can be represented as follows,

$$\begin{aligned}
\text{Minimize} \quad & J = f_{ode}\left(\overline{x}, t, \overline{u}, \overline{d}\right) \\
\textbf{Subject to:} & \\
\text{Dynamic constraints:} \quad & \dot{\overline{x}} = f_{ode}\left(\overline{x}, t, \overline{u}, \overline{d}\right) \\
\text{Time:} \quad & t_{lb} \leq t \leq t_{ub} \\
\text{State variables:} \quad & \overline{x}_{lb} \leq \overline{x} \leq \overline{x}_{ub} \\
\text{Dynamic controls:} \quad & \overline{u}_{lb} \leq \overline{u} \leq \overline{u}_{ub} \\
\text{Design parameters:} \quad & \overline{d}_{lb} \leq \overline{d} \leq \overline{d}_{ub} \\
\text{Initial boundary constraints:} \quad & \overline{g}_{0,lb} \leq g_0\left(\overline{x}_0, t_0, \overline{u}_0, \overline{d}_0\right) \leq \overline{g}_{0,ub} \\
\text{Final boundary constraints:} \quad & \overline{g}_{f,lb} \leq g_f\left(\overline{x}_f, t_f, \overline{u}_f, \overline{d}_f\right) \leq \overline{g}_{f,ub} \\
\text{Path constraints:} \quad & \overline{p}_{f,lb} \leq p_f\left(\overline{x}, t, \overline{u}, \overline{d}\right) \leq \overline{p}_{f,ub}
\end{aligned} \tag{2.3}$$

Regarding the number of optimization variables, trajectory optimization problems can be classified in either single or multi-objective. The most common objective is to minimize the cost of the flight by taking into account both the fuel cost and the time-related costs. Depending on the requirements and objectives of the mission it is worth noting that it exists trade-off between speed, accuracy, flexibility, robustness and optimality as shown in table 2.1.

| Criteria | Feature |
|---|---|
| Speed | Computational time to provide a solution |
| Accuracy | Level of closeness to reality |
| Flexibility | Range of applicability to other scenarios |
| Robustness | Level of numerical stability and sensitivity to the first guess |
| Optimality | Level of closeness to the optimal solution |

Table 2.1: Performance Criteria for Trajectory Optimization [14]

## 2.2 Numerical Approaches

In the context of optimization problems, numerical approaches refer to computational methods used to find approximate solutions. These approaches are employed when analytical solutions are not readily available. Numerical approaches can be divided in two well-known methods: indirect methods and direct methods. For a fundamental background in the associated methodologies, the reader should refer to [5], [9], [30].

### 2.2.1 Indirect methods

An indirect optimization method is a technique for solving optimization problems where the necessary and sufficient conditions for optimality are constructed analytically and then numerically. The goal is to solve transform the problem into a multi-point boundary value problem (MPBVP) that results from applying the Pointryagin Minimum Principle (PMP) [29]. These methods typically involve iteratively updating the solution based on derivative information to converge towards the optimal point. A brief conceptual depiction of their implementation is provided hereby. For a more comprehensive review, the reader is referred to [9], [14] and [7].

- **Indirect single shooting**: It is an iterative technique in which a set of unknown initial conditions are made. At every iteration, these initial conditions are adjusted until the difference between the known and the desired terminal conditions does not overcome a threshold.
- **Indirect Multiple shooting**: It follows the same principle as the single shooting. However, in this case, the time interval is broken up into N+1 subintervals. Additionally, continuity conditions have to be applied at the boundary of each interval. This method ameliorates the robustness of the indirect single-shooting
- **Indirect Collocation**: The states and costate differential equations are transformed into a set of discrete defect constraints. Then, the unknown discretized states and costates are modified to drive the defect constraints to zero and meet the boundary conditions.

### 2.2.2 Direct methods

A direct optimization method, is an approach that does not rely on derivative information, such as gradients or Hessians to guide the search for the optimal solution. Instead, they explore the objective function by sampling points in the search space and evaluating their corresponding function values. Among them it is possible to distinguish the following methods. Direct methods transform the original problem via discretization of the control and state functions on a time grid to a non-linear programming (NLP) problem. The NLP is then numerically solved using well-known optimization techniques [30]. For a more in depth explanation, the reader is referred to [5] and [14].

- **Differential inclusion**: Only the state variables are discretized over a predefined time-grid. This method apply inequality constraints on the rates of change of the states. The discretized states are updated until the inequality constraints are satisfied and the cost function minimized. Nevertheless, this technique can present numerical instability.

- **Direct single shooting**: Like indirect single shooting method, the state is propagated from $t_0$ to $t_f$. Additionally it discretizes the control on a specified time-grid, and solve for the discretized controls that optimize the cost function. Then, the control parameters are updated at each iteration by comparing the desired terminal conditions with the obtained ones.
- **Direct multiple shooting**: The principle followed by this method is the same as the aforementioned indirect multiple shooting. Thus, each segment is denoted with the values of the state at the beginning of each subinterval and the discretized controls being unknown in the optimization. In every iteration, the optimization parameters are updates until the cost is minimized and the constraints satisfied.
- **Direct collocation**: it discretizes both the control and state variable time histories. As well, the dynamic system equations are transformed into discrete defect constraints, which relate the values at the beginning of the subinterval to the values at the end.

| | **Flexibility** | **Robustness** | **Optimality** |
|---|---|---|---|
| Indirect Methods | Low | Low | High |
| Direct Methods | High | High | Low |

Table 2.2: Numerical approaches performance

## 2.3 Solutions Approaches

Hitherto, methods for solving Non Linear Programming (NLP) problems have been classified taking into account the technique for solving the optimization problem. However, it is important, as well, to introduce a classification based on the nature of the solution. Extensive information about solution approaches can be found in [5] and [14].

- **Deterministic methods:** These methods will always produce the same output under the same initial conditions. They are based on phenomena that follow a predictable chain of events.
- **Heuristic methods:** The search is performed without requiring gradient information. Thus, these methods do not guarantee to be optimal, perfect, or rational, but nevertheless sufficient for reaching an immediate, short-term objective. Heuristic methods can be used to speed up the process of finding a satisfactory trajectory.
- **Stochastic methods:** It involves introducing randomness or probability distributions in the solution process. They are particularly useful when dealing with black box cost functions where the Jacobian is not available and the problem is uncertain. Some examples are genetic algorithms [20] or particle swarm optimization[28].

| | **Flexibility** | **Robustness** | **Optimality** |
|---|---|---|---|
| Deterministic Methods | Low | High | High |
| Heuristic Methods | High | Low | Low |
| Stochastic Methods | High | High | Low |

Table 2.3: Numerical solutions performance

## 2.4 Exploring Surrogate Model Techniques

Surrogate models are frequently used to replace high-fidelity simulations with faster approximations. However, in this study, the introduction of surrogate models is a matter of developing a data-driven approach aiming to generate more realistic solutions and substitute the analytical models. The selection of the surrogate model method lies on the characteristics that define the database such as the size, the dimension (number of inputs and outputs) and the non-linearity.

Commonly used surrogate models for medium size and low dimension datasets include Radial Basis Functions, Polynomial Regression Models or Kriging,

- **Polynomial Regression Model:** it fits a polynomial equation to the data points. These models are simple to implement but they are limited to linear or low-order nonlinear relationships [25].
- **Kringing (Gaussian Process Regression):** it is a probabilistic model that assumes a Gaussian process providing predictions with uncertainty estimates. It is highly accurate with uncertainty quantification. However it is computationally expensive for large datasets [18].
- **Radial Basis Functions Model (RBF):** it is based on radial basis functions as weighted sum to approximate the objective function. The model can capture nonlinear relationships whereas the selection of the parameters can be challenging and performance can degrade with high-dimensional data [2].

Nevertheless, when the size of the database increases, the performance of the aforementioned methods drops. In order to be able to effectively deal with big dataset, Machine Learning (ML) algorithms are the best candidates. ML algorithms are computational methods that allow computers to learn patterns and relationships from data. They identify patterns in the input data and use them to make predictions or decisions on unseen data. Commonly used machine learning algorithms are Artificial Neural Networks (ANNs), Support Vector Machines (SVMs) or Random Forest regression.

- **Artificial Neural Networks (ANNs):** there are layers of interconnected neurons to approximate complex functions. It is capable of capturing highly complex and nonlinear relationships although it requires a large amount of data to train it [34].
- **Support Vector Machine (SVMs):** it finds a hyperplane to separate data into different categories. It is effective in high-dimensional spaces and robust to overfitting. Nevertheless, it is sensitive to the choice of kernel and parameters [24].
- **Random Forest Regression:** it builds multiple decision tress and averages their predictions to reduce the variance. It offers high predictive accuracy and robustness against overfitting due to the averaging of multiple trees. Conversely, the model can be computational intensive and present memory allocation problems with large datasets and numerous trees [26].

## 2.5 Exploring Initial Guess Determination Techniques

A proper initial guess can drastically reduce the convergence time and improve the solution quality of the optimization process. Some widely spread methods for the initial guess generation are historical flight data analysis to derive initial guesses for similar flight conditions. Private databases or internet portals such as *Flight Aware* [1] allow to intensively seek for similar former real routes. By implementing these data as initial guess, the likelihood of convergence and the computational time significantly improve.

Also, there are other approaches in which machine learning techniques are used to predict a close optimal solution, so it can then be introduced in a gradient based optimizer to find the global minimum. The key challenge of this procedure is to gather the necessary data to train the machine learning method.

# 3 Workspace

Capgemini Engineering (formerly known as Altran Technologies) is part of the Capgemini group, focused on engineering solutions, disruptive technologies and R&D. By taking advantage of in-depth engineering and digital knowledge, Capgemini Engineering supports their partners bringing together the digital and physical world, accelerating the transition to the sustainable Intelligent Industry. This goal is executed by the company's more than 52000 employees in more than 30 countries, across various sectors, such as aeronautics, aerospace, industrial engineering, rail, communications, health and automotive. Inside the company, the Technology Engineering Center (TEC), located in Toulouse, has more than 2000 engineers and scientists spread into many different domains, including Mechanical, Fluid and Thermal, Electrical Engineeiring, Acoustics, Flight Science, Telecommunications and many others. Additionally, it is also home to the TEC R I Department, where more than 100 researchers work on internal projects, ranging from future urban mobility to sustainable energy and industries.

Inside the TEC and its Physical Mechanical Engineering (PME) perimeter is the Acoustics and Optimization Pole, working to reduce noise in many applications as well as carry out optimization process such as the design of new aircrafts complying with the ever-increasing regulatory demands. Among the pole's capabilities is the know-how in different fields such as aeroacoustics, vibroacoustics and overall aircraft optimization.

The OPTIMIND project is a cutting-edge research initiative aimed at defining complex systems through multidisciplinary optimization. This project encompasses several domains, including aerodynamic and performance optimization, which focuses on enhancing aerodynamic efficiency, trajectory optimization, and failure prevention. The aeroelastic optimization domain addresses structural modeling, load management, and blade/wing shape optimization to prevent whirl flutter. The aeroacoustic optimization domain works to minimize noise reflection and direct acoustic propagation along preferred paths. Life cycle optimization applies MDO workflows to product life cycle analysis, aiming to enhance sustainability and reduce unwanted byproducts. Additionally, the project includes vibroacoustic optimization, focusing on reducing cabin noise and developing advanced vibroacoustic models.

# 4 Methodology

## 4.1 Aircraft Flight Dynamics

The following methodology aims to formulate the equations of motion of the aircraft in order to be able to establish the optimal control problem and the approach that is to be done to find a proper solution. However, before starting with their formulation, it is necessary to define the reference frames that will be used in the problem: the topocentric inertial system, the local horizon axes system, the wind axes system, and the body axes system. Once the reference systems are defined, the equations governing the vehicle's motion will be presented: a total of 6 equations with 6 unknowns and various control variables.

### 4.1.1 Reference System

As aforementioned, to address the equations affecting the vehicle, it is essential to establish the different reference systems that will participate in the problem. First, an inertial system is to be defined from which the relative wind and vehicle reference systems will be determined.

#### 4.1.1.1 Earth Axes System

The Earth is used as an inertial system. The earth axes system E($O_E$, $x_E$, $y_E$, $z_E$) is defined as follows:

For the definition of this reference system T(O, x, y, z), the flat Earth hypothesis is assumed. Thus, the Earth's surface is flat, and any reference system fixed on it (topocentric) is inertial. The axes are defined as follows:

- O (origin): any point on the surface.
- x-axis: North direction.
- y-axis: East direction.
- z-axis: Completes a right-handed triad (pointing downwards).

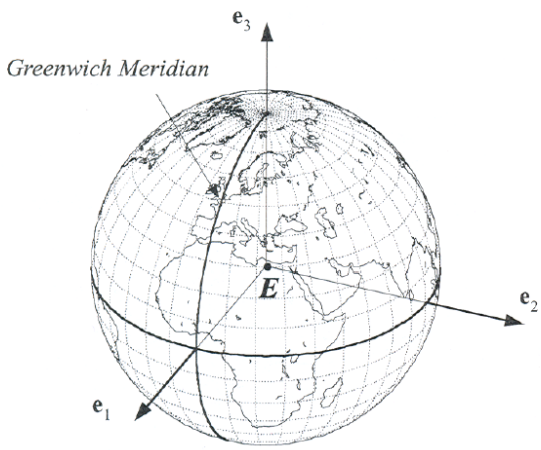


Figure 4.1: Earth axes system [31]

#### 4.1.1.2 Geographic Axes System

The geographic axis system G($O_G$, $x_G$, $y_G$, $z_G$) is defined as follows (see Figure 1.3):

- $O_G$ (origin): center of mass of the Earth;
- $x_G$-axis: in the direction and sense of the position vector $\vec{r}$
- $y_G$-axis: contained in the equatorial plane, orthogonal to ($x_G$), and directed towards the east;

- $z_G$-axis: completes a right-handed triad.

Local horizontal plane: plane that passes through point M where the vehicle is located and is orthogonal to the position vector $\vec{r}$ (that is, orthogonal to the $x_G$ axis).

The orientation between the geographic axis system with respect to the Earth axis system can be defined with the following angles,

1. Latitude ($\lambda$): angle between the vector $\vec{r}$ and the equatorial plane, positive when heading north.
2. Longitude ($\theta$): angle between the projection of $\vec{r}$ onto the equatorial plane and the axis $x_E$, positive to the East.

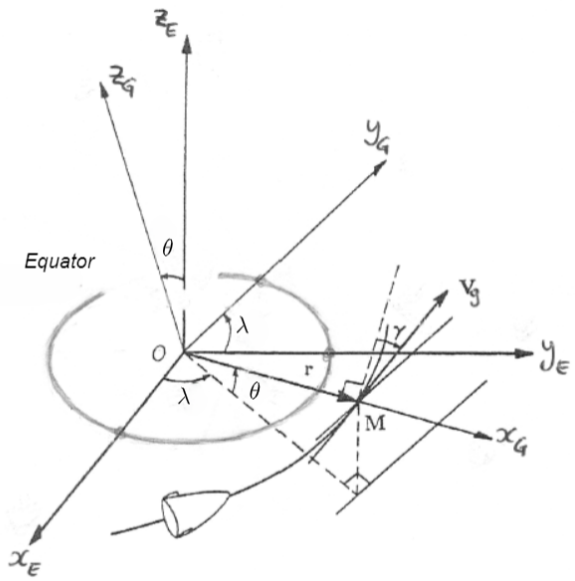


Figure 4.2: Geographic axes system [31]

Thus, the transformation matrix is obtained, firstly, with a rotation of angle $\theta$ around the $z_E$ axis and, secondly, with rotation of angle $\lambda$ around the $y_G$ axis, where the transformation matrix is,

$$[Tr]^{GE} = [Tr]^{GX}[Tr]^{XE} = \begin{pmatrix} \cos\lambda & 0 & \sin\lambda \\ 0 & 1 & 0 \\ -\sin\lambda & 0 & \cos\lambda \end{pmatrix} \begin{pmatrix} \cos\theta & \sin\theta & 0 \\ -\sin\theta & \cos\theta & 0 \\ 0 & 0 & 1 \end{pmatrix} = \begin{pmatrix} \cos\lambda\cos\theta & \cos\lambda\sin\theta & \sin\lambda \\ -\sin\lambda & \cos\lambda & 0 \\ -\sin\lambda\cos\theta & -\sin\lambda\sin\theta & \cos\lambda \end{pmatrix} \tag{4.1}$$

#### 4.1.1.3 Local Horizon Axes System

The local horizon axes system H($O_h$, $x_h$, $y_h$, $z_h$) arises from the translation of the Topocentric Inertial System to the vehicle's center of mass. The local horizon axes also form an inertial system as their orientation always coincides with the axes T(O, x, y, z).

- $O_h$ (origin): Vehicle's center of mass.
- $x_h$-axis: North direction.
- $y_h$-axis: East direction.
- $z_h$-axis: Completes a right-handed triad (pointing downwards).

#### 4.1.1.4 Wind Axes System

The wind axes system W($O_w$, $x_w$, $y_w$, $z_w$) is associated with the vehicle's movement relative to the air.

- $O_w$ (origin): Vehicle's center of mass.
- $x_w$-axis: Has the same direction and sense as the aerodynamic velocity vector $\vec{V}$.
- $z_w$-axis: Contained in the vehicle's symmetry plane and directed downwards for a zero flight path angle ($\gamma$).
- $y_w$-axis: Completes a right-handed triad.

The orientation of the wind axes concerning the local horizon axes can be defined through three angles:

1. Flight path angle ($\gamma$): the angle formed by the aerodynamic velocity vector $\vec{V}$ and the local horizon plane. It is considered positive when the vector points upwards following the sign criterion used in the literature [31]. It can be depicted in figure 4.3
2. Heading angle ($\chi$): the angle formed by the projection of the aerodynamic velocity vector $\vec{V}$ onto the local horizon plane with the north direction. It is considered positive towards the east (clockwise).
3. Bank angle ($\mu$): the angle formed by the $y_w$-axis with the local horizon plane. For the sign criterion.

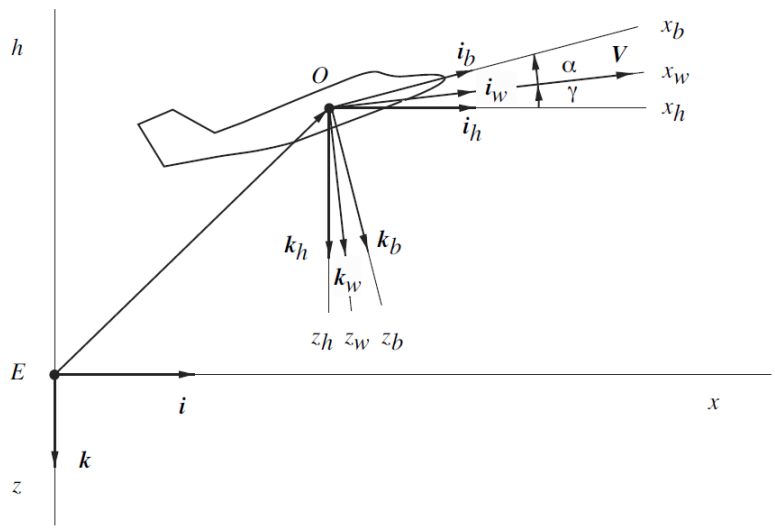


Figure 4.3: Local horizon axes system and wind axes [17]

To formulate the equations, a rotation matrix is needed to transform magnitudes from one system to another. The transformation $H \longrightarrow W$ is obtained from the local horizon axes through a rotation by angle $\chi$ around the $z_h$-axis, followed by a rotation by angle $\gamma$ around the $y'$-axis, and then a rotation by angle $\mu$ around the $x''$-axis.

$$[Tr]^{WH} = [Tr]^{WX''} \cdot [Tr]^{X''X'} \cdot [Tr]^{X'H} = \begin{pmatrix} 1 & 0 & 0 \\ 0 & \cos\mu & \sin\mu \\ 0 & -\sin\mu & \cos\mu \end{pmatrix} \cdot \begin{pmatrix} \cos\gamma & 0 & -\sin\gamma \\ 0 & 1 & 0 \\ \sin\gamma & 0 & \cos\gamma \end{pmatrix} \cdot \begin{pmatrix} \cos\chi & \sin\chi & 0 \\ -\sin\chi & \cos\chi & 0 \\ 0 & 0 & 1 \end{pmatrix} =$$

$$= \begin{pmatrix} \cos\gamma\cos\chi & \cos\gamma\sin\chi & -\sin\gamma \\ \sin\mu\sin\gamma\cos\chi - \cos\mu\sin\chi & \sin\mu\sin\gamma\sin\chi + \cos\mu\cos\chi & \sin\mu\cos\gamma \\ \cos\mu\sin\gamma\cos\chi + \sin\mu\sin\chi & \cos\mu\sin\gamma\sin\chi - \sin\mu\cos\chi & \cos\mu\cos\gamma \end{pmatrix} \tag{4.2}$$

#### 4.1.1.5 Body Axes System

The body axes system B($O_b$, $x_b$, $y_b$, $z_b$) moves together with the vehicle and is defined as follows:

- $O_b$ (origin): Vehicle's center of mass.
- $x_b$-axis: In the same direction as the vehicle's symmetry axis.
- $z_b$-axis: Contained in the vehicle's symmetry plane and directed downwards for a zero flight path angle ($\gamma$).
- $y_b$-axis: Completes a right-handed triad.

The orientation of the body axes relative to the wind axes can be defined through two angles:

1. Sideslip angle ($\beta$): the angle formed by the aerodynamic velocity vector $\vec{V}$ with the $x_b z_b$ plane, positive when the air enters from the right.
2. Angle of attack ($\alpha$): the angle formed by the projection of the aerodynamic velocity vector $\vec{V}$ onto the $x_b z_b$ plane and the $x_b$-axis.

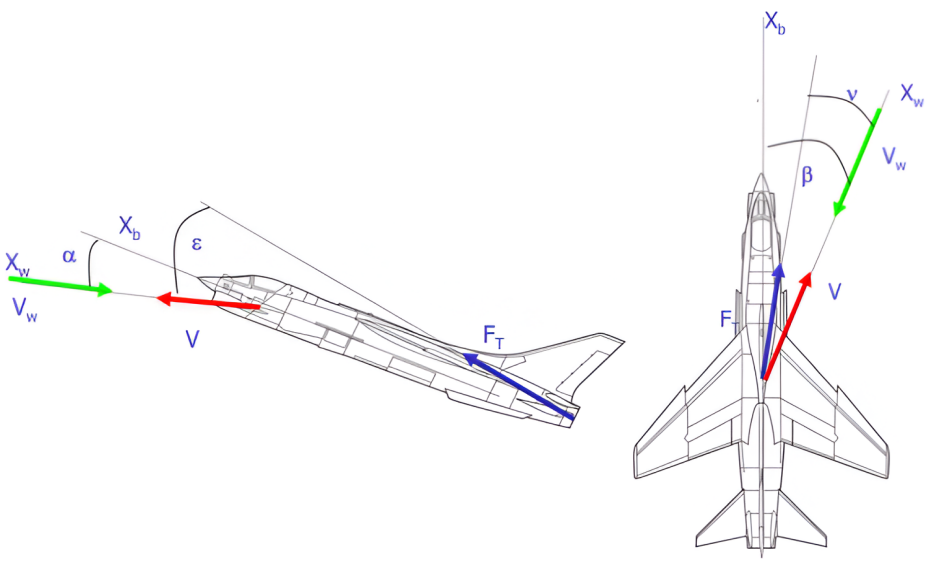


(a) Definition of $\alpha$ (b) Definition of $\beta$

Figure 4.4: Body frame with respect to wind frame [4]

The transformation $W \longrightarrow B$ is obtained from the wind axes through a rotation by angle $\beta$ around the $z_w$-axis, followed by a rotation by angle $\alpha$ around the $y_b$-axis, resulting in the transformation matrix:

$$[Tr]^{BW} = \begin{pmatrix} \cos\alpha\sin\beta & -\cos\alpha\sin\beta & -\sin\alpha \\ \sin\beta & \cos\beta & 0 \\ \sin\alpha\cos\beta & -\sin\alpha\sin\beta & \cos\alpha \end{pmatrix} \tag{4.3}$$

It can be defined as well to more angles with respect to the wind axis. Thus, the orientation of the engines in the aircraft adds the following angles:

1. Thrust sideslip angle ($\nu$): the angle formed by the projection of aerodynamic velocity vector $\vec{V}$ onto the $x_b y_b$ plane and the thrust projection onto the $x_b y_b$ plane, positive when the air enters from the right.
2. Thrust angle of attack ($\epsilon$): the angle formed by the projection of the aerodynamic velocity vector $\vec{V}$ onto the $x_b z_b$ plane and the thrust projection onto the $x_b z_b$ plane.

where:

$$\epsilon = \epsilon_0 + \alpha \tag{4.4}$$

being $\epsilon_0$ the nominal direction between the axial's aircraft body frame and the engine. If not specified, the value of $\epsilon_0$ will be equal to zero.

Furthermore, the orientation of the body axes relative to the local horizon axes is given by three angles:

1. Pitch angle ($\Theta$): the angle formed by the $x_b$-axis with the local horizon plane, positive downwards. This sign criterion, different from

   the one typically used, is more intuitive for this problem.

2. Yaw ($\psi$): the angle formed by the projection of the $x_b$-axis onto the local horizon plane with the north direction, positive towards the east.

3. Roll angle ($\phi$): the angle formed by the $y_b$-axis with the local horizon plane.

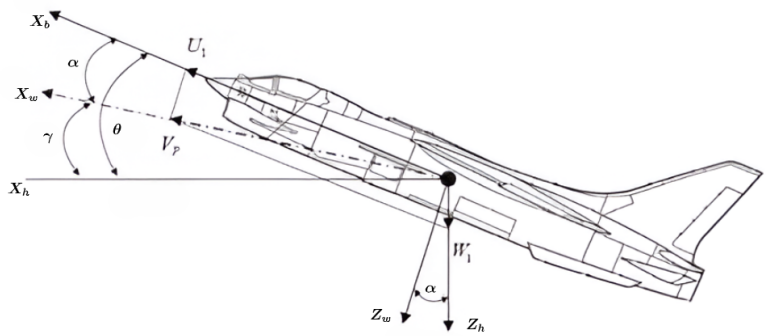


(a) Definition of $\Theta$

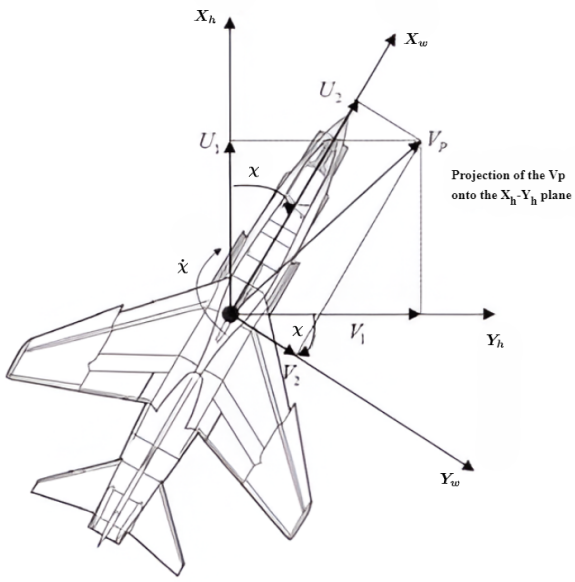


(b) Definition of $\psi$

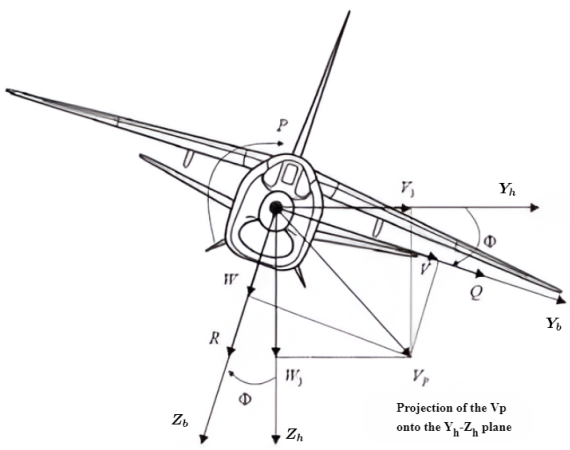


(c) Definition of $\phi$

Figure 4.5: Body frame with respect to wind frame [4]

The transformation $H \longrightarrow B$ is obtained from the local horizon axes through a rotation by angle $\psi$ around the $z_h$-axis, followed by a rotation by angle $\Theta$ around the $y'$-axis, and then a rotation by angle $\phi$ around the $x''$-axis.

$$[Tr]^{BH} = [Tr]^{BX''}[Tr]^{X''X'}[Tr]^{X'H} = \begin{pmatrix} 1 & 0 & 0 \\ 0 & \cos\phi & \sin\phi \\ 0 & -\sin\phi & \cos\phi \end{pmatrix} \cdot \begin{pmatrix} \cos\Theta & 0 & \sin\Theta \\ 0 & 1 & 0 \\ -\sin\Theta & 0 & \cos\Theta \end{pmatrix} \cdot \begin{pmatrix} \cos\psi & \sin\psi & 0 \\ -\sin\psi & \cos\psi & 0 \\ 0 & 0 & 1 \end{pmatrix} =$$

$$= \begin{pmatrix} \cos\Theta\cos\psi & \cos\Theta\sin\psi & \sin\Theta \\ -\cos\phi\sin\psi + \sin\phi\sin\Theta\cos\psi & \cos\phi\cos\psi + \sin\phi\sin\Theta\sin\psi & -\sin\phi\cos\Theta \\ -\sin\phi\sin\psi - \cos\phi\sin\Theta\cos\psi & \sin\phi\cos\psi - \cos\phi\sin\Theta\sin\psi & \cos\phi\cos\Theta \end{pmatrix} \tag{4.5}$$

### 4.1.2 Equations of motion

Once the necessary reference system have been defined, the equation of motion which describes the behaviour of the aircraft will be presented. The motion of the vehicle is defined at each instant by its position, velocity and mass as,

$$\begin{aligned} \left(\frac{d\vec{r}}{dt}\right)_I &= \vec{V}_I \\ m\left(\frac{d\vec{V}_I}{dt}\right)_I &= \vec{F}_A + \vec{F}_T + m\vec{g} \\ \frac{dm}{dt} &= -\eta \cdot T \end{aligned} \tag{4.6}$$

being $\vec{r}$ the position vector, $t$ the time, $V_I$ the inertial velocity of the vehicle, $m$ the mass, $\vec{F}_A$ and $\vec{F}_T$ the aerodynamic and propulsive force respectively and $c$ the fuel mass flow. Thus, it is a system composed by 7 differential equations, 3 for the position, 3 for the velocity and the mass. It is worth remarking that the sub-index, in this case $I$, after the parenthesis denotes the reference system with respect to which the magnitude is being measured.

The aforementioned equations are based on an inertial system. However, because the Earth rotates at a constant angular velocity, the Earth axes reference frame is non-inertial. According to a theorem in Classical Mechanics, for a fixed reference frame $F$ and a rotating reference frame $M$ with angular velocity $\vec{\omega}_{MF}$ relative to $F$, the relationship between the time derivatives of a vector $\vec{A}$ in both systems is given by:

$$\left(\frac{d\vec{A}}{dt}\right)_F = \left(\frac{d\vec{A}}{dt}\right)_M + \vec{\omega}_{MF} \times \vec{A} \tag{4.7}$$

Then, the geocentric inertial system and Earth axes are described as,

$$\begin{aligned} \left(\frac{d\vec{r}}{dt}\right)_I &= \left(\frac{d\vec{r}}{dt}\right)_E + \vec{\omega} \times \vec{r} \\ m\left(\frac{d\vec{V}_I}{dt}\right)_I &= \left(\frac{d\vec{V}_g}{dt}\right)_E + 2\vec{\omega} \times \vec{V}_g + \omega \times (\omega \times \vec{r}) \end{aligned} \tag{4.8}$$

The terms $2\vec{\omega} \times \vec{V}_g$ and $\omega \times (\omega \times \vec{r})$ are the Coriolis and centrifugal acceleration respectively. However, this accelerations can be neglected as the rotational angular velocity is $7.27 \cdot 10^{-5}\ rad/s$ and it only has effect at a major scale (e.g. meteorology). Thus, as a conclusion, for this problem the Earth axes system (E) will be considered as an inertial system.

#### 4.1.2.1 Kinematic equations

The kinematic equations are composed by 3 differential equations which describe the movement of the vehicle within the three axis. Given that,

$$\left(\frac{d\vec{r}}{dt}\right)_E = \left(\frac{d\vec{r}}{dt}\right)_H + \vec{\omega}_{HE} \times \vec{r} = \vec{V} \tag{4.9}$$

being $E$ the Earth axes frame, $H$ the local horizon frame, $\vec{V}$ the inertial velocity and $\vec{\omega}_{HE}$ the angular velocity of the local horizon reference system with respect to the Earth axes reference system. This vector can be described as,

$$\vec{\omega}_{HE} = \dot{\theta}\vec{k}_E - \dot{\lambda}\vec{j}_G \tag{4.10}$$

In order to be able to work with equation 4.9 it is necessary to use the same reference system for every term, in this case the local horizon reference system (H).

$$\left[\left(\frac{d\vec{r}}{dt}\right)_H\right]^H + [\vec{\omega}_{HE}]^H \times [\vec{r}]^H = \left[\vec{V}\right]^H \tag{4.11}$$

Thus, the variables in the local horizon system are defined as follows,

$$[r]^H = \begin{pmatrix} 0 \\ 0 \\ -r \end{pmatrix} \tag{4.12}$$

$$\left[\left(\frac{d\vec{r}}{dt}\right)_H\right]^H = \begin{pmatrix} 0 \\ 0 \\ -\dot{r} \end{pmatrix} \tag{4.13}$$

the velocity can be easily defined in the wind axes reference system $W$, to then carry out the transformation from wind to local horizon system using the matrix $[Tr]^{HW}$. To obtain the rotation matrix the orthogonality property is used,

$$[Tr]_{WH} \cdot [Tr]^T_{WH} = I \quad \text{so that,} \quad [Tr]^{-1}_{WH} = [Tr]^T_{WH} \tag{4.14}$$

where the suprascript $T$ denotes the transpose matrix, and the supra-index *-1* the inverse matrix. Thereby, using the transpose of matrix 4.2 yields the desired rotation matrix, in fact, $[Tr]_{HW} = [Tr]^T_{WH}$.

$$[V]^W = \begin{pmatrix} V \\ 0 \\ 0 \end{pmatrix} \quad [V]^H = [Tr]^{HW}[V]^W = \begin{pmatrix} V\cos\gamma\cos\chi \\ V\cos\gamma\sin\chi \\ -V\sin\gamma \end{pmatrix} \tag{4.15}$$

On the other hand, the angular velocity has to be transformed step to step. Firstly, the vector is rotated to the geographic system and then, to the local horizon system.

$$[\omega_{GE}]^G = \dot{\theta}[Tr]^{GE}[k_E]^E - \dot{\lambda}[j_G]^G = \begin{pmatrix} \sin\lambda\dot{\theta} \\ -\dot{\lambda} \\ \cos\lambda\dot{\theta} \end{pmatrix} \tag{4.16}$$

$$[\omega_{HE}]^H = [Tr]^{HG}[\omega_{GE}]^G = \begin{pmatrix} \cos\lambda\dot{\theta} \\ -\dot{\lambda} \\ \sin\lambda\dot{\theta} \end{pmatrix} \tag{4.17}$$

Once every term from equation 4.11 is obtained with respect to the local horizon reference system it is possible to define the scalar kinematic equations,

$$\begin{aligned} (R_T + h)\frac{d\lambda}{dt} &= V\cos\gamma\cos\chi \\ (R_T + h)\cos\lambda\frac{d\theta}{dt} &= V\cos\gamma\sin\chi \\ \frac{dh}{dt} &= V\sin\gamma \end{aligned} \tag{4.18}$$

where it has been taken into account the relation $r = R_T + h$, being $R_T$ the radius of the Earth and constant.

Finally, it is possible to add the atmospheric wind to the kinematic equations. The creation of the wind model is described in section 4.2.3. In this study only the wind in the horizontal plane of the aircraft will be taken into account, meaning that the upwards and downwards wind will be neglected. Additionally, it has been assumed that the wind is stationary, meaning that the values of u and v components will not change with time along the trajectory. Finally, it is worth remarking that the u and v components are not correlated making it possible to work with them independently. Thus, the wind vector can be determined in the local horizon system as,

$$[v_w]^H = \begin{pmatrix} u_w \\ v_w \\ 0 \end{pmatrix} \tag{4.19}$$

being straightforward to add the axial and transversal wind components to the kinematic equations.

$$\begin{aligned} (R_T + h)\frac{d\lambda}{dt} &= V\cos\gamma\cos\chi + v_w \\ (R_T + h)\cos\lambda\frac{d\theta}{dt} &= V\cos\gamma\sin\chi + u_w \\ \frac{dh}{dt} &= V\sin\gamma \end{aligned} \tag{4.20}$$

#### 4.1.2.2 Dynamic equations

The dynamic equations are defined using Newton's second law. It determines the behaviour of the system under certain forces over time. They are composed by 3 differential equations which yields the three velocity components. Thus, using the relation from Classical Mechanics between two systems with a relative motion between one another and Newton's second law,

$$\left(\frac{d\vec{V}}{dt}\right)_E = \left(\frac{d\vec{V}}{dt}\right)_W + \vec{\omega}_{WE} \times \vec{V} = \frac{1}{m}\vec{F}_{A,T} + \vec{g} \tag{4.21}$$

being $E$ the Earth axes, $W$ the wind axes, $\vec{F}_{A,T}$ the aerodynamic and propulsive forces and $\vec{g}$ the gravity force vector. Conversely to the kinematic equations, every term of equation 4.21 is going to be projected onto the wind axes,

$$\left[\left(\frac{d\vec{V}}{dt}\right)_W\right]^W + [\vec{\omega}_{WE}]^W \times \left[\vec{V}\right]^W = \frac{1}{m}\left[\vec{F}_{A,T}\right]^W + [\vec{g}]^W \tag{4.22}$$

$$\left[\left(\frac{d\vec{V}}{dt}\right)_W\right]^W = \begin{pmatrix} \dot{V} \\ 0 \\ 0 \end{pmatrix} \tag{4.23}$$

The gravity term is defined using the rotation matrix $[Tr]^{WH}$ from equation 4.2 in order to carry out the transformation between local horizontal and wind axes.

$$[g]^H = \begin{pmatrix} 0 \\ 0 \\ g \end{pmatrix} \qquad [g]^W = [Tr]^{WH}[g]^H = \begin{pmatrix} -g\sin\gamma \\ g\cos\gamma\sin\mu \\ g\cos\gamma\cos\mu \end{pmatrix} \tag{4.24}$$

The angular velocity $\vec{\omega}_{WE}$ is determined by the sum of two relative rotational velocities, where $\vec{\omega}_{HE}$ has been previously defined in equation 4.17.

$$\vec{\omega}_{WE} = \vec{\omega}_{WH} + \vec{\omega}_{HE} \tag{4.25}$$

Thereby, the angular velocity of the local horizontal system with respect to the wind axes can be determined as follows,

$$\vec{\omega}_{WH} = \dot{\chi}\vec{k}_h + \dot{\gamma}\vec{j}_{x'} + \dot{\mu}\vec{i}_w \tag{4.26}$$

where $h$ denotes the local horizon system, $x'$ the auxiliary frame created to define the wind axes and $w$ the wind axes system. Thereupon, it is needed to rewrite the vector onto the same reference system, in this case $W$.

$$[\omega_{WH}]^W = \dot{\chi}\,[Tr]^{WH}\,[k_h]^H + \dot{\gamma}\,[Tr]^{WX'}\,[j_{x'}]^{X'} + \dot{\mu}\,[i_w]^W = \begin{pmatrix} -\dot{\chi}\sin\gamma + \dot{\mu} \\ \dot{\chi}\cos\gamma\sin\mu + \dot{\gamma}\cos\mu \\ \dot{\chi}\cos\gamma\cos\mu + \dot{\gamma}\sin\mu \end{pmatrix} \tag{4.27}$$

Then, summing the result with the previously calculated angular velocity properly rotated onto wind axes,

$$[\omega_{WE}]^W = [\omega_{WH}]^W + [Tr]^{WH}\,[\omega_{HE}]^H \tag{4.28}$$

Thus, the cross product from equation 4.22 is computed as,

$$[\vec{\omega}_{WE}]^W \times \left[\vec{V}\right]^W \approx \begin{pmatrix} 0 \\ V(\dot{\chi}\cos\gamma\cos\mu - \dot{\gamma}\sin\mu) \\ -V(\dot{\chi}\cos\gamma\sin\mu + \dot{\gamma}\cos\mu) \end{pmatrix} \tag{4.29}$$

where the terms with order of magnitude $V^2/r$ have been neglected with respect to $g$. Finally, the dynamic equations are defined.

$$\begin{aligned} \frac{dV}{dt} &= \frac{1}{m}(F_{A,T})_{x_w} - g\sin\gamma \\ V\cos\gamma\frac{d\chi}{dt} &= \frac{1}{m}\left[(F_{A,T})_{y_w}\cos\mu - (F_{A,T})_{z_w}\sin\mu\right] \\ V\frac{d\gamma}{dt} &= -\frac{1}{m}\left[(F_{A,T})_{y_w}\sin\mu - (F_{A,T})_{z_w}\cos\mu\right] - g\cos\gamma \end{aligned} \tag{4.30}$$

being the force in every wind axis,

$$[F_{A,T}]^W = \begin{pmatrix} T\cos\epsilon\cos\nu - D \\ T\cos\epsilon\sin\nu - Q \\ -(L + T\sin\epsilon) \end{pmatrix} \tag{4.31}$$

where for this problem, $\epsilon_0 = 0$ so that $\epsilon = \alpha$, $\nu = 0$ and the lateral component of the drag is null, $Q = 0$. Thus, the aerodynamic and propulsive forces are simplified as,

$$[F_{A,T}]^W = \begin{pmatrix} T\cos\alpha - D \\ 0 \\ -(L + T\sin\alpha) \end{pmatrix} \tag{4.32}$$

**Assumptions**

1. **Neglect of Coriolis and centrifugal acceleration in the atmosphere.**
2. **Symmetric flight:** vectors $\vec{V}$ and $\vec{T}$ are contained onto the same symmetry plane. Thus, $\beta = \nu = Q = 0$.
3. **Nominal direction between the axial's aircraft body frame and engine ($\epsilon_0$) is null.**
4. **Stationary wind is assumed along the whole trajectory.**
5. **Only transversal and axial wind is taken into account, no downward/upward direction.**

**Summary**

$$\begin{aligned}
(R_T + h)\frac{d\lambda}{dt} &= V\cos\gamma\cos\chi + v_w \\
(R_T + h)\cos\lambda\frac{d\theta}{dt} &= V\cos\gamma\sin\chi + u_w \\
\frac{dh}{dt} &= V\sin\gamma \\
m\frac{dV}{dt} &= T\cos\alpha - D - mg\sin\gamma \\
mV\cos\gamma\frac{d\chi}{dt} &= (L + T\sin\alpha)\sin\mu \\
mV\frac{d\gamma}{dt} &= (L + T\sin\alpha)\cos\mu - mg\cos\gamma \\
\frac{dm}{dt} &= -\eta\cdot T
\end{aligned} \tag{4.33}$$

## 4.2 Performance Model

### 4.2.1 BADA user manual

BADA is a collection of ASCII files which specifies operation performance parameters, airline procedure parameters and performance summary tables for 295 aircraft types. This information is designed for use in trajectory simulation and prediction algorithms within the domain of Air Traffic Management (ATM). This document describes the mathematical models on which the data is based and specifies the format of the files which contain the data [12]. Thus, the atmosphere, aerodynamic, thrust and fuel consumption model of this master thesis are defined following the BADA user manual.

#### 4.2.1.1 Standard Atmosphere

The equations used by BADA for the standard atmosphere are summarized below. These equations are based on the International Standard Atmosphere (ISA).

1. **Determination of the tropopause.**

$$h_{trop} = 11000 + \frac{1000\Delta\tau_{ISA}}{6.5} \tag{4.34}$$

Here, the tropopause altitude, $h_{trop}$, is specified in meters. $\Delta\tau_{ISA}$ is the temperature difference from the International Standard Atmosphere (ISA). That is, the temperature at sea level, $\tau_0$, would be:

$$\tau_0 = (\tau_0)_{ISA} + \Delta\tau_{ISA} \quad with \quad (\tau_0)_{ISA} = 288.15K \tag{4.35}$$

For standard atmosphere conditions, $\Delta\tau_{ISA} = 0$, the tropopause is at 11000 meters altitude.

2. **Determination of Temperature.**

Above the tropopause, the temperature is constant:

$$\tau_{trop} = 216.65K \tag{4.36}$$

Below the tropopause, the temperature is calculated as a function of altitude as follows:

$$\tau = \tau_0 - \frac{6.5h}{1000} \tag{4.37}$$

Here, the altitude $h$ is specified in meters.

3. **Determination of Air Density.**

Above the tropopause, the air density is determined as,

$$\rho = \rho_{trop} \cdot e^{-\left(\frac{g}{R \cdot \tau_{trop}}\right)(h - h_{trop})} \tag{4.38}$$

whereas, below the tropopause, the air density is a calculated as a function of the temperature as follows,

$$\rho = \rho_0 \left(\frac{\tau}{\tau_0}\right)^{-\frac{g}{K_T R}-1} \quad where \quad -\frac{g}{K_T R} - 1 = 4.25864 \tag{4.39}$$

being $\rho_0$ the air density at sea level, $\rho_0 = 1.225 kg/m^3$.

The air density $\rho$ is in $kg/m^3$, the temperature in Kelvin, the altitude in meters. As well, R denotes the real gas constant for air ($R = 287.04m^2/Ks^2$), g is the gravitational acceleration ($g = 9.81m/s^2$) and $k_T$ is the ISA temperature gradient with the altitude below the tropopause, ($k_T = -0.0065K/m$).

4. **Determination of Pressure.**

   Above the tropopause, the pressure is determined as,

$$p = p_{trop} \cdot e^{-\left(\frac{g}{R \cdot \tau_{trop}}\right)(h-h_{trop})} \tag{4.40}$$

   whereas, below the tropopause, the pressure is a calculated as a function of the temperature as follows,

$$p = p_0 \left(\frac{\tau}{\tau_0}\right)^{-\frac{g}{K_T R}} \quad where \quad -\frac{g}{K_T R} = 5.25791 \tag{4.41}$$

   being $p_0$ the pressure at sea level, $p_0 = 101325Pa$.

   The air density $p$ is in Pascals ($Pa$), the temperature in Kelvin, the altitude in meters. As well, R denotes the real gas constant for air ($R = 287.04m^2/Ks^2$), g is the gravitational acceleration ($g = 9.81m/s^2$) and $k_T$ is the ISA temperature gradient with the altitude below the tropopause, ($k_T = -0.0065K/m$).

5. **Determination of Speed of Sound.** Above the tropopause the speed of sound is constant,

$$a_{trop} = \sqrt{\gamma R \tau_{trop}} = 295.07m/s \tag{4.42}$$

   being $\gamma$ the isentropic expansion coefficient for air $\gamma = 1.4$, $R = 287.04m^2/Ks^2$ and $\tau_{trop} = 216.65K$.

   Below the tropopause, the temperature is calculated as a function of the temperature.

$$a = 340.29\sqrt{\frac{\tau}{\tau_0}} \tag{4.43}$$

   where $\tau_0 = 288.15K$.

#### 4.2.1.2 Aerodynamics

Under nominal conditions, the drag coefficient, $C_D$, is specified as a function of the lift coefficient $C_L$ as follows:

$$C_D = C_{D0,CR} + C_{D2,CR} \times (C_L)^2 \tag{4.44}$$

Equation 4.44 is valid for all situations except for approach and landing, where other drag coefficients are to be used. However, the approach and landing phases will not be tackled in this study. For further information [12].

The drag force (in Newtons) is then determined from the drag coefficient in the standard manner:

$$D = \frac{C_D \cdot \rho \cdot V_{TAS}^2 \cdot S}{2} \tag{4.45}$$

where: $\rho$ is the air density $\left(kg/m^3\right)$ $S$ is the wing reference area $\left(m^2\right)$ $V_{\text{TAS}}$ is the true airspeed ($m/s$).

Finally, the lift force, $L$, is formulated as follows,

$$L = \frac{C_L \cdot \rho \cdot V_{TAS}^2 \cdot S}{2} \tag{4.46}$$

The terms $C_{D0,CR}$, $C_{D2,CR}$ and $C_L$ are specified in the OPF (Operations Performance File) file of the aircraft type provided by Eurocontrol.

#### 4.2.1.3 Engine Thrust

The BADA model provides coefficients that allow the calculation of the following thrust levels: maximum climb, nominal climb, maximum take-off, maximum cruise and descent. For this study only the maximum climb, maximum cruise and descent thrust will be defined. For further information the reader should refer to [12].

The thrust is calculated in Newtons and includes the contribution for all engines. The subsections below provide the equations for each of the three formerly mentioned thrust conditions.

1. **Maximum Climb.** The maximum climb thrust at standard atmosphere conditions, $(T_{maxclimb})_{ISA}$ , is calculated in Newtons as a function of the engine type (in this study jet engine), the altitude above sea level, $h$, in feet, true air speed, $V_{TAS}$, in knots and temperature deviation from standard atmosphere, $\Delta T_{ISA}$, in degrees Celsius. The equation for the maximum climb thrust for a jet is described as,

$$(T_{\text{max climb}})_{\text{ISA}} = C_{\text{Tc1}} \times \left(1 - \frac{h}{C_{\text{Tc2}}} + C_{\text{Tc3}} \times h^2\right) \tag{4.47}$$

   For all engine types, the maximum climb thrust is corrected for temperature deviations from standard atmosphere, $\Delta T_{\text{ISA}}$, in the following manner:

$$T_{\text{max climb}} = (T_{\text{max}\,climb})_{\text{ISA}} \times (1 - C_{\text{Tcs}} \cdot (\Delta T_{\text{ISA}})_{\text{eff}}) \tag{4.48}$$

   where

$$(\Delta T_{\text{ISA}})_{\text{eff}} = \Delta T_{\text{ISA}} - C_{\text{Tc4}} \tag{4.49}$$

   with the limit:

$$0.0 \leq (\Delta T_{\text{ISA}})_{\text{eff}} \times C_{\text{Tc5}} \leq 0.4 \tag{4.50}$$

   The coefficients $C_{Tc,1}$, $C_{Tc,2}$, $C_{Tc,3}$, $C_{Tc,4}$ and $C_{Tc,5}$ are defined in the OPF file of the aircraft type provided by Eurocontrol.

2. **Maximum Cruise Thrust.**

   The normal cruise thrust is by definition set equal to drag ($T = D$). However, the maximum amount of thrust available in cruise situations is limited. The maximum cruise thrust is calculated as a ratio of the maximum climb thrust given in section 3.7.1, that is:

$$(T_{\text{cruise}})_{\text{Max}} = C_{\text{Tcr}} \times T_{\text{max climb}} \tag{4.51}$$

   The coefficient $C_{\text{Tcr}}$ is currently uniformly set to 0.95 for all aircraft.

3. **Descent Thrust.**

   Descent thrust is calculated similarly to cruise thrust, with different correction factors used for high and low altitude, and approach and landing configurations

$$T_{\text{des}} = C_{\text{Tdes}} \times T_{\text{max climb}} \tag{4.52}$$

   In this study all the correction factors are considered equal to 1.

#### 4.2.1.4 Fuel Consumption

The thrust-specific fuel consumption, $\eta$, in $kg/min/kN$, is specified as a function of true airspeed, $V_{TAS}$ (knots), for the jet engine. The nominal fuel flow, $f_{nom}$ ($kg/minute$), can then be calculated as,

$$\eta = C_{f1} \times \left(1 + \frac{V_{TAS}}{C_i}\right) \tag{4.53}$$

with:

$$f_{\text{nom}} = \eta \times T \tag{4.54}$$

These expressions are used in all flight phases except during cruise and for descent/idle conditions.

Minimum fuel flow, $f_{\text{min}}$, corresponding to idle thrust or descent conditions for jet engines, is specified in $kg/min$ as a function of altitude above sea level, $h$ (ft), that is:

$$f_{\text{min}} = C_B \left(1 - \frac{h}{C_f}\right) \tag{4.55}$$

Cruise fuel flow, $f_{cr}$, is calculated using the thrust-specific fuel consumption $\eta$ and a cruise fuel flow factor, $C_{fcr}$:

$$f_{cr} = \eta \times T \times C_{fcr} \tag{4.56}$$

For the moment, the cruise fuel flow correction factor has been established for a number of aircraft. This factor has been set to 1 (one) for all the other aircraft models.

### 4.2.2 Surrogate model

A surrogate model is a mathematical function used to approximate the behaviour of a complex system. Its purpose is to substitute complex and computationally expensive models by providing faster and simpler solutions. This feature is particularly important for trajectory optimization given the vast number of iterations and simulations required. Also, in this context, it serves as a more realistic approach of the problem. For instance, the performance of an aircraft's powerplant is influenced by the specific engine model and the operational conditions. Thus, having a dataset that captures engine thrust across a wide range of conditions and creating a sufficiently accurate surrogate model, will leverage the problem to a more realistic approach rather than using standard propulsion equations.

The python library used to create the propulsion and fuel consumption surrogate models is *Surrogate Modelling Toolbox SMT* [32] and [6]. The reason why this python package has been selected is its focus on derivatives which are a matter of paramount importance in gradient-based optimization. The derivatives of interest in *SMT* toolbox are: derivatives of predicted outputs with respect to the inputs, derivatives of training outputs and derivatives of predicted outputs with respect to training outputs.

#### 4.2.2.1 Kringing method

The Kringing method, also known as Gaussian Process Regression (GPR), is a spread surrogate modelling technique. It is a statistical method that interpolates the value of a random field at an unsampled point using known data points. It is assumed that the distance between data points can be used to predict unknown values. Furthermore, it provides an estimation of uncertainty in the prediction as depicted in figure 4.6, which is useful in optimization and decision-making.

The reason why Kringing method has been selected among the other methods is the fact that it performs exceptionally well with small to medium datasets. It does not require large amounts of data to generate accurate models. Its accuracy decreases in very large datasets due to computational expense. Additionally, Kringing is highly capable of modelling complex and non-linear relationship in the data, in fact, it is particularly suited for modelling smooth and continuous systems such as the propulsion and fuel consumption models. Finally, it provides not only the predictions but also the measure of the uncertainty associated with each prediction which can be included in the optimization to explore design spaces efficiently.

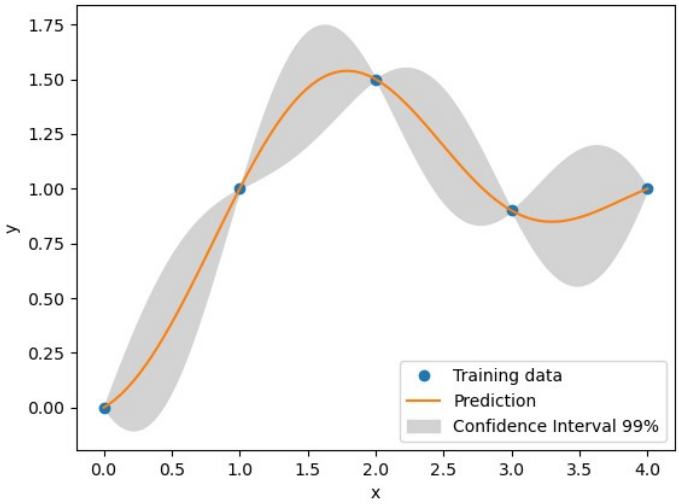


Figure 4.6: Example of Kringing method [10]

Kringing method will be used to define the propulsion and specific fuel consumption models. The datasets used to trained these models are not large and its behaviour is not highly-linear. For that reason, it is expected that the performance of the aforementioned surrogate modelling method will be sufficiently accurate.

#### 4.2.2.2 Neural Networks

When the size of the database used to train the models is considerably big, the performance of the methods in *SMT* library is very poor. This is the case of the dataset of the atmospheric wind presented in section 4.2.3 with more than three millions items. Hence, the most efficient way to tackle this vast amount of data is using machine learning techniques such as neural networks.

Neural networks are computational models inspired by the human brain's structure. As it is not the main subject of this thesis, this section will not delve deeply into all the principles behind neural networks. Thus, a brief and accurate definition of its structure, how do they work and its training process will be presented. For further information of neural networks the reader should refer to [11].

Neural networks composed of interconnected layers of nodes, where each node processes input data and passes its output to the next layer. The network learns by adjusting the weights of connections based on the error of

its predictions. The learning process can be carried out using backpropagation and optimization techniques to minimize the error. Some key characteristics are,

1. Layers: The structure of a neural network is define by an input layer that receives the raw data. After this input layer, there are intermediate layers known as hidden layers. Finally the output layer produces the final output of the network
2. Neurons or nodes: it is the basic unit of computation in a neural network. Each layer is composed by a specific number of nodes. The node receives the input, process it using an activation function and passes the result to the next layer.
3. Weights: it involves emphasizing the contribution of particular aspects of a set of data over others. The goal is to find the right weights during the training process.
4. Activation functions: they introduced non-linearity. Without activation functions, a neural network would essentially be a linear model, regardless of how many layers it has. The used activation function in this study is ReLU (Rectified Linear Unit).
5. Biases: additional parameters added to the weighted sum of inputs in a node, allowing the model to fit the data better by shifting the activation function.
6. Regularization: neural networks can sometimes learn noise from the training dataset. Regularization techniques such as dropout or L2 regularization mitigate this issue. However, further on, it will be shown for the wind model that regularization and smoothing is not desirable.

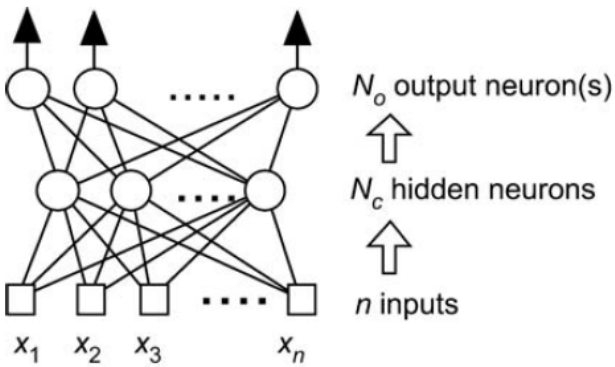


Figure 4.7: A neural network with $n$ inputs, a layer of $N_c$ hidden neurons and $N_o$ output neurons [11]

Now that a brief description of how a neural network is structured it is time to determine how to tackle the training process. During the training, an optimization process is undertaken in which the model's weight and biases are adjusted to minimize the loss function. The loss function quantifies how far off the predictions of the model are from the actual values. The optimization algorithm used in this thesis, and one of the most popular, is Adam (Adaptive Moment Estimation). The key features of Adam are the adaptive learning rate based on the historical gradients and the bias correction terms.

Finally, among all the methods, neural networks have been chosen due to the fact that they excel at capturing complex, non-linear relationships as it occurs in wind patterns. Hence, although it is often found abruptness in wind behaviour it is possible to maintain smoothness in the model which is crucial for computing the derivatives using finite differences. However, to be able to capture more accurately the wind changes, more layers and nodes must be added and an optimization of the parameters must be carried out. The selected library in python to develop neural networks is *pytorch* [27].

### 4.2.3 Introduction of wind effects

The wind can affect considerably the performance of the aircraft. In this study, only the wind in the local horizon plane is taking into account, meaning that only axial and transversal winds will affect the trajectory. The introduction of this atmospheric effects will influence in fuel consumption and time of flight. It is worth noting one important phenomena located in the upper layers of the troposphere called jet streams. It is a consequence of solar radiation and the Coriolis force due to Earth's rotation. The strongest jet streams are the polar jets found between latitudes 30° and 60° and altitudes from 30000 to 40000 feet, affecting the cruise phase. It can reach up speeds of more than 442 km/h [22], although it has a mean velocity of around 150 km/h and the direction is from west to east. For that reason it is important in route optimization to avoid or to use the jet stream in order to save fuel and time.

In order to build the wind model the data used is the Copernicus Data Store called ERA5 [16]. ERA5 provides hourly estimates for a large number of atmospheric, ocean-wave and land-surface quantities and is updated daily with a latency of about 5 days. For this case, it is only used the u component and v component of the wind in the pressure range between 1000 hPa and 250 hPa. Following the International Standard Atmosphere (ISA) it corresponds to altitudes from 100 to 14400 meters. Hence, it is possible to extract the data for sub-regions which is convenient if only short or medium range flight routes are being calculated. For this master thesis the sub-region chosen is within the range $[30°N,\ 70°N]$, $[30°W,\ 30°E]$ and the subregion within the range $[30°N,\ 70°N]$, $[80°W,\ 10°E]$.

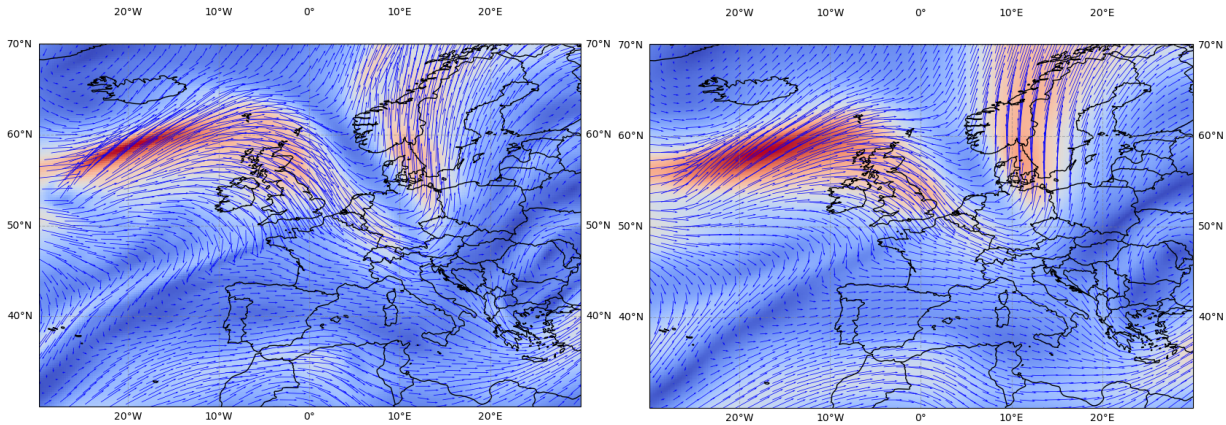


(a) Wind vector map from Copernicus dataset [16]

(b) Wind vector map from Deep Neural Network model

Figure 4.8: Wind comparison corresponding to an altitude of 10362 m.

Figure 4.8 shows the atmospheric wind at 500 hPa. As formerly mentioned, the presence of the polar jet stream is noticeable particularly between Iceland and the British-Irish Isles. Also, as depicted in 4.9b the Neural Network wind model replicates the wind behaviour with smoother patterns with difficulties when sudden changes in wind appear, although maintaining a high level of accuracy available in table 4.1.

| | R2 score | RMSE |
|---|---|---|
| **u component** | 0.9733 | 1.670 |
| **v component** | 0.9685 | 1.6417 |

Table 4.1: Evaluation of u and v component of the wind.

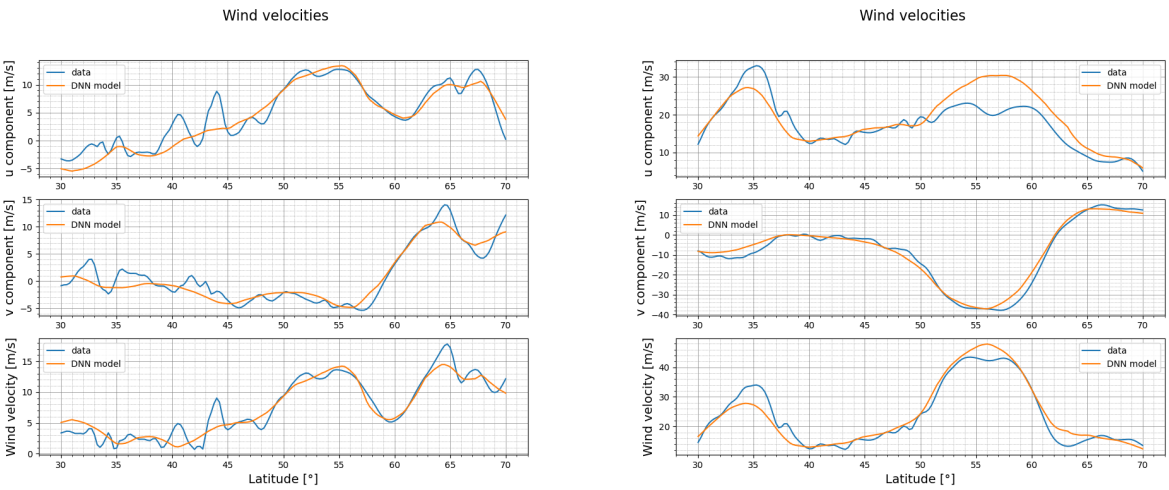


(a) Wind profile for a pressure of 850 hPa

(b) Wind profile for a pressure of 250 hPa

Figure 4.9: Wind comparison along different latitudes at a constant longitude and height.

## 4.3 Formulation of Aircraft Trajectory Optimization Problem

An optimal control problem is composed of an objective function that is desired to be maximized or minimized subjected to dynamic, boundary and path constraints, as presented in section 2. The dynamic constraints are the equations of motion of the system and determine its evolution with time whereas the boundary and path constraints are limitations imposed to the optimal solution. Thus, the aim of an optimal control problem is to find the right values of the control variables for each time step in order to extremize an objective while satisfying some constraints.

There are several ways to tackle an optimal control problem. In this chapter, the optimal control transcriptions used in this study will be presented and justified as well as the method utilized to solve the optimization problem. Finally, the whole problem setting will be defined.

### 4.3.1 Problem definition

1. **Discussion of the equations of motion.** The previously defined system of equations 4.33 determines the evolution and behaviour of the aircraft. Thus, the equations of motions involve the following variables,

$$\lambda(t),\ \theta(t),\ V(t),\ \chi(t),\ \gamma(t),\ m(t),\ throttle(t),\ \alpha(t),\ \mu(t) \tag{4.57}$$

The variables $\lambda$, $\theta$, $h$, $V$, $\chi$, $\gamma$ and $m$ whose derivatives appear in equation 4.33 are called state variables. The remaining variables $\alpha$, $throttle(t)$ and $\mu$ whose derivatives not appear are known as control variables.

Actually, the pilot controls the fuel flow rate to the engine using the throttle to increase or decrease the power, and thus, the thrust. Hence, the pitch of the aircraft is controlled by deflecting the elevator which is a control surface located in the horizontal stabilizer, in the back of the plane, which rotates upward or downward the aircraft, changing the angle of attack $\alpha$. Furthermore, the roll is controlled by deflecting the ailerons. They are aerodynamic surfaces situated in the wings which are deflected asymmetrically to create a roll moment and induced a bank angle $\mu$ in the aircraft.

The number of mathematical degrees of freedom of the presented system is three which is aligned with the number of independent control variables available for the pilot.

Additionally, in aircraft performance it is convenient to use the lift coefficient as a variable rather than the angle of attack. The convenience arises when the angle of attack and the drag are influence by the following variables,

$$\alpha = \alpha(h,\ V,\ L) \quad D = D(h,\ V,\ L) \tag{4.58}$$

The lift coefficient is the result of the nondimensionalization of the lift force. Following a dimensional analysis,

$$CL = \frac{L(h,\ V,\ \alpha)}{\frac{1}{2}\rho V^2 S} \quad \text{where} \quad CL = CL(\alpha) \tag{4.59}$$

being $\rho$, $V$ and $S$ the air density, the velocity and the characteristic surface respectively. Thus, the lift coefficient is only dependent on the angle of attack $\alpha$. Hence, equation 4.58 is rewritten as,

$$\alpha = \alpha(CL) \quad D = D(CL) \tag{4.60}$$

Finally the state and control variables of the problem are described in table 4.2. The objective of the optimal control problem will be to find the proper values for $CL$, $throttle$, $\mu$, so that an objective is extremize while the variables $\lambda$, $\theta$, $h$, $V$, $\chi$, $\gamma$ and $m$ meet the constraints.

| | Symbol | Name | Magnitude | Bounds |
|---|---|---|---|---|
| State variables | $\lambda$ | latitude | degree | [-90°, 90°] |
| | $\theta$ | longitude | degree | [-180°, 180°] |
| | $h$ | altitude | m | [100 m, 12000 m] |
| | v | velocity | m/s | [75 m/s, -] |
| | $\gamma$ | flight path angle | degree | [-30°, 30°] |
| | $\psi$ | heading angle | degree | [-180°, 180°] |
| | $m$ | mass | kg | [OWE, MTOW] |
| Control variables | $CL$ | lift coefficient | None | [0, 1.5] |
| | $throttle$ | throttle of the engine | None | [0, 1] |
| | $\mu$ | bank angle | degree | [-30°, 30°] |

Table 4.2: State and control variables

2. **Cost function**

The cost function or objective function is the mathematical expression that evaluates the behaviour and performance of the problem in terms of a specific criteria. For instance, in trajectory optimization is frequent to use the duration of the flight or the fuel consumed along the flight. The aim of an optimization problem is to find the extremes of this cost function either a global maximum or global minimum while satisfying the rest of the constraints.

In aeronautics, it is widespread among the airlines the use of Cost Index. The fundamental rationale of the cost index concept is to achieve minimum trip cost by means of a trade-off between operating costs per hour and incremental fuel burn. Thus, the cost index is used to take into account the relationship between fuel and time-related costs [3].

$$C = C_F \cdot \Delta F + C_T \cdot \Delta T + C_C \tag{4.61}$$

where

$$\begin{aligned} C &: \text{total cost} && [€] \\ C_F &: \text{cost of fuel per kg} && [€/\text{kg}] \\ C_T &: \text{cost of time per minute of flight} && [€/\text{min}] \\ C_C &: \text{fixed costs} && [€] \\ \Delta F &: \text{Trip fuel} && [\text{kg}] \\ \Delta T &: \text{Flight duration} && [\text{s}] \end{aligned} \tag{4.62}$$

Hence, removing the fixed costs and dividing the equation by the cost of fuel per kg $C_F$ it yields,

$$J = \Delta F + CI \cdot \Delta T \quad with \quad CI = \frac{C_T}{C_F} \tag{4.63}$$

The cost function is denoted as $J$ and the cost index as $CI$. The value of the cost index usually goes from 0 to 99, although it depends on the FMS (Flight Management System) [3].

Time related costs contain the sum of several components, the hourly maintenance cost, the flight crew and cabin crew cost per flight hour and the marginal depreciation or leasing costs (for instance the cost of ownership or aircraft rental).

With time-related costs, the faster the aircraft is flown, the more money is saved. However, if the aircraft is flown faster to reduce time-related costs, fuel burn increases and money will be lost in turn. On the

other hand, to avoid over-consumption of fuel, the aircraft should be flown more slowly. Thus the cost index value is a trade-off selection that is made by each airline depending on their priorities.

For the A320 family the following cost index ranges are presented,

| Time Cost($ /min) / Fuel Cost ($ /kg) | **Low (<10)** | **Medium (10<to<15)** | **High (>15)** |
|---|---|---|---|
| **Low (<0.7)** | 40 | 60 | 80 |
| **Medium (0.7<to<0.9)** | 30 | 45 | 60 |
| **High (>0.9)** | 25 | 40 | 50 |

Table 4.3: A320 family cost index [3]

3. **Phase definition and constraints**

The trajectory is composed of three different phases, climb, cruise and descent. In this study the take off, approach and landing are not taking into account. Thus, the climb is the process by which the aircraft reach the cruise altitude at a range between 29000 ft and 39000 ft for an A320. The climb is characterized by a quick ascent. Then, the cruise is generally the larger phase of the trajectory where a constant altitude is maintained if no deviation is needed due to air traffic management. Finally, the descent, is carried out in iddle mode which means that the thrust is minimal. This phase is constrained with a maximum vertical velocity and a maximum velocity. As well, following the same pattern as the aforementioned climbing phase, the descent phase is short.

Hence, in order to properly define the boundaries and limitations of each phase, different boundary and path constraints have been added to the optimization problem. The boundary constraints aim to delimit, in this case, the final values of some variables such as the altitude, the latitude or the longitude. On the other hand, the path constraints determine the ranges that the state and control variables must satisfy.

| | **Location** | **Value** |
|---|---|---|
| h | final | cruise altitude |

Table 4.4: Climb boundary constraints

| | **Lower bound** | **Upper bound** |
|---|---|---|
| h | departure altitude | cruise altitude |
| mach | 0.3 | 0.82 |
| throttle | 0.03 | 0.95 |
| CL | 0.0 | 1.5 |
| mu | $-20.0°$ | $20.0°$ |

Table 4.5: Climb path constraints

| | **Location** | **Value** |
|---|---|---|
| h | final | cruise altitude |

Table 4.6: Climb boundary constraints

| | Lower bound | Upper bound |
|---|---|---|
| $\dot{h}$ | 0 | 0 |
| mach | 0.6 | 0.82 |
| throttle | 0.03 | 0.9 |
| CL | 0.0 | 1.5 |
| mu | $-20.0°$ | $20.0°$ |

Table 4.7: Cruise path constraints

| | Location | Value |
|---|---|---|
| h | final | arrival altitude |
| $\gamma$ | final | $-3.0°$ |
| $\chi$ | final | runway course |
| $\lambda$ | final | arrival airport latitude |
| $\theta$ | final | arrival airport longitude |

Table 4.8: Descent boundary constraints

| | Lower bound | Upper bound |
|---|---|---|
| $\dot{h}$ | $-12.7$ m/s | - |
| h | 275 ft | - |
| mach | 0.35 | 0.82 |
| throttle | 0.03 | 0.03 |
| CL | 0.0 | 1.5 |
| mu | $-20.0°$ | $20.0°$ |

Table 4.9: Descent path constraints

### 4.3.2 Optimal control transcriptions

Solving optimal control problems using classical techniques is typically a matter of finding continuous control function that moves a system towards the desired state while extremizing some objective [13].

In order to be able to solve these problems using non linear optimizers, it is necessary to find a way to discretize this continuous problem into a form that can be solved by nonlinear optimizers. This way of splitting the continuous problem is called transcription. The main forms of direct transcription are collocation and explicit shooting.

Collocation-based optimal control methods, also referred to as pseudospectral methods, are implicit approaches. In these methods, the entire trajectory of the system's state and control inputs is proposed at specific time points. Then, an evaluation is done on how well this proposed trajectory satisfies the system's governing ODE, with any discrepancies referred to as defects. By iteratively adjusting the states, controls, and time intervals, these defects can be minimized to zero, indicating that the proposed trajectory is a valid solution to the ODE given the control inputs and time span.

In contrast, explicit shooting involves using an explicit numerical integration method to evolve the initial state over the specified time period based on the given controls. This integration process inherently corrects any defects in the trajectory.

As a general aspect, the design variable vector and the constraint vector can be considerably larger for the implicit collocation techniques, depending on the size of the state vector and the number of discrete points in time.

Given that the design variable and constraint vectors are significantly larger in implicit collocation problems, one might assume they would be slower to solve than explicit shooting methods. However, this assumption is incorrect.

In single shooting methods, the value of a state at a later time potentially depends on all preceding events, resulting in a Jacobian matrix of derivatives for these state values that is lower triangular.

Conversely, for implicit collocation techniques, the state within one integration segment is independent of events outside that segment. the Jacobian matrix is much sparser. This sparsity offers two main advantages.

First, the derivatives can be computed more efficiently. Second, certain optimizers can leverage the sparsity of Jacobian matrices to achieve significantly better performance compared to those working with dense matrices. These factors enable collocation techniques to be orders of magnitude faster than explicit shooting methods.

For that reason, given the number of size of the state vector and the number of discrete points needed for the trajectory optimization, the collocation technique will be applied for this study.

| | **Implicit collocation method** | **Single shooting method** |
|---|---|---|
| Size of variable and constraint vector | larger | shorter |
| Jacobian matrix of the derivatives | sparse | low triangular |
| Sparsity of the matrix can be increased | yes | no |

Table 4.10: Stability margins of the controlled launcher

### 4.3.3 Collocation

The principle behind the collocation method involves selecting a finite-dimensional space of potential solutions, typically polynomials up to a specific degree, and identifying a set of points within the domain known as collocation points. The optimal solution is then determined by ensuring that it satisfies the given equation precisely at these collocation points.

Regarding that over portions of the trajectory, the state and its first derivative with respect to time are continuous the value of the state at any point throughout the trajectory can then be inferred by interpolating the collacated polynomial. In this case an implicit collocation will be applied.

Solving this trajectory implicitly means estimating the state values along the path. While power series polynomial coefficients could be used, they can vary significantly based on the curve's shape, making numerical scaling challenging. Instead, Lagrange interpolating polynomials are generally preferred, where the actual values at various points serve as the implicit variables. This approach simplifies scaling, and the implicit variables are more intuitive, making it easier to provide an initial estimate.

### 4.3.4 Determination of initial guess

Much of the time, an initial guess is required to solve an optimal control problem. An initial guess is a starting point for the optimization solver to start iterating from. A good start can make the problem converge in fewer iterations, while a poor one can make it crash in the first iteration. Thus, the selection of a proper initial guess is crucial for the convergence of the problem and the computational time.

The objectives from section 1.1 determine the need of generating a strategy to compute accurate and automatic initial guesses so that the inputs introduced by the user are only focused on the departure and arrival airport and not also on the initial guess of every state and control variable. This feature will facilitate the study of different routes and setting without the concern of setting up new initial guesses every time.

The method selected to determine the initial guess consists on introducing real flight data of the same route that is desired to be optimized. In the majority of the cases, real routes are not far away from the optimal path when the objective function is the cost of the flight (generally taking into account the cost of fuel and the cost

of time). The website that has been used for this data acquisition is *Flight Aware* [1]. In *Flight Aware* it is possible to select the destination and arrival airport, as well as the type of aircraft among the available ones. Furthermore, it can be selected both previous or scheduled flights, although only the past flight are of interest in this context.

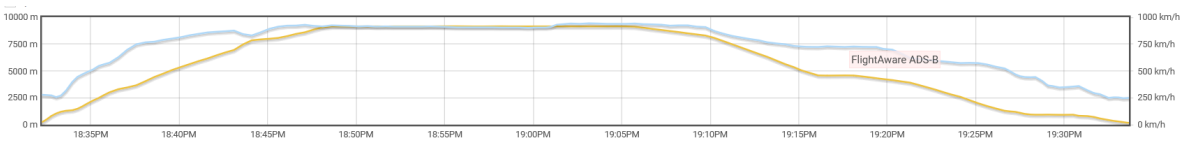


| Horaire (CEST) | Latitude | Longitude | Cap | nœuds | km/h | mètres | Taux | Centre d'informations |
|---|---|---|---|---|---|---|---|---|
| lun. 18h32:15 **Départ (TLS) @ lundi 18h32:15 CEST** | | | | | | | | FlightAware ADS-B (TLS / LFBO) |
| lun. 18h32:15 | 43.6265 | 1.3689 | ↘ 143° | 150 | 278 | 221 | | FlightAware ADS-B (TLS / LFBO) |
| lun. 18h32:31 | 43.6180 | 1.3778 | ↘ 143° | 149 | 275 | 488 | 1.100 ↑ | FlightAware ADS-B (TLS / LFBO) |
| lun. 18h32:47 | 43.6089 | 1.3872 | ↘ 143° | 147 | 272 | 808 | 1.029 ↑ | FlightAware ADS-B (LFBR) |
| lun. 18h33:03 | 43.6010 | 1.3950 | ↘ 146° | 138 | 256 | 1.036 | 729 ↑ | FlightAware ADS-B (LFCL) |
| lun. 18h33:19 | 43.5919 | 1.4035 | ↘ 146° | 146 | 270 | 1.196 | 457 ↑ | FlightAware ADS-B (LFMW) |
| lun. 18h33:36 | 43.5823 | 1.4127 | ↘ 145° | 170 | 315 | 1.288 | 223 ↑ | FlightAware ADS-B (TLS / LFBO) |
| lun. 18h33:58 | 43.5654 | 1.4287 | ↘ 150° | 215 | 398 | 1.341 | 281 ↑ | FlightAware ADS-B (LFCL) |
| lun. 18h34:15 | 43.5477 | 1.4306 | ↓ 194° | 240 | 444 | 1.471 | 623 ↑ | FlightAware ADS-B (TLS / LFBO) |
| lun. 18h34:31 | 43.5333 | 1.4167 | ↙ 229° | 252 | 467 | 1.684 | 873 ↑ | FlightAware ADS-B (TLS / LFBO) |
| lun. 18h34:48 | 43.5269 | 1.3900 | ← 269° | 264 | 489 | 1.951 | 902 ↑ | FlightAware ADS-B (TLS / LFBO) |
| lun. 18h35:08 | 43.5355 | 1.3576 | ← 302° | 277 | 513 | 2.240 | 809 ↑ | FlightAware ADS-B (LFCL) |
| lun. 18h35:27 | 43.5549 | 1.3374 | ↖ 335° | 295 | 546 | 2.477 | 823 ↑ | FlightAware ADS-B (TLS / LFBO) |
| lun. 18h35:43 | 43.5759 | 1.3269 | ↑ 346° | 302 | 560 | 2.720 | 865 ↑ | FlightAware ADS-B (TLS / LFBO) |
| lun. 18h36:04 | 43.6045 | 1.3205 | ↑ 353° | 311 | 576 | 3.010 | 681 ↑ | FlightAware ADS-B (LFMW) |
| lun. 18h36:34 | 43.6493 | 1.3131 | ↑ 351° | 339 | 628 | 3.299 | 450 ↑ | FlightAware ADS-B (TLS / LFBO) |
| lun. 18h37:04 | 43.6977 | 1.3017 | ↑ 350° | 376 | 697 | 3.459 | 360 ↑ | FlightAware ADS-B (LFCL) |
| lun. 18h37:35 | 43.7524 | 1.2889 | ↑ 350° | 404 | 748 | 3.665 | 568 ↑ | FlightAware ADS-B (LFBR) |
| lun. 18h38:06 | 43.8095 | 1.2754 | ↑ 350° | 414 | 766 | 4.046 | 757 ↑ | FlightAware ADS-B (LFDH) |
| lun. 18h38:36 | 43.8681 | 1.2616 | ↑ 350° | 417 | 772 | 4.435 | 701 ↑ | FlightAware ADS-B (LFDH) |
| lun. 18h39:06 | 43.9257 | 1.2479 | ↑ 350° | 426 | 789 | 4.747 | 648 ↑ | FlightAware ADS-B (TLS / LFBO) |
| lun. 18h39:36 | 43.9854 | 1.2337 | ↑ 350° | 433 | 801 | 5.083 | 617 ↑ | FlightAware ADS-B (TLS / LFBO) |

Figure 4.10: Toulouse-Paris Charles de Gaulle flight chart [1]

As depicted in figure 4.10 the flight data that can be retrieved is the latitude, longitude, velocity, altitude and time.

A function has been created to obtain automatically from the Internet the formerly mentioned variables and transform it into an array to be introduced as an initial guess as presented in figure 4.11. Furthermore, it splits up the array into the three differences phases (climb, cruise and descent). This function uses Selenium and Beautiful Soup packages for python.

However the initial guess has to be introduced to every state and control variable of the problem as defined in table 4.2. Using the function that retrieves the data from *Flight Aware* website, it is possible to provide the initial guess of $\lambda$, $\theta$, $h$, $v$, and $\psi$. Thus, it is needed to define manually the rest of the variables which are $\gamma$, $m$, $CL$, *throttle* and $\mu$. Except from the mass, these variables are not critical features of the problem and normally they do not change considerably from one problem to another or it does not heavily affect the initial guess.

The mass is determined taking into account the mean fuel consumption in $kg/s$ for each phase.

$$\begin{aligned} m_{climb} &= m_{ini} - 1.1 \cdot t_{climb} \\ m_{cruise} &= m_{climb} - 0.6 \cdot t_{cruise} \\ m_{descent} &= m_{cruise} - 0.1 \cdot t_{descent} \end{aligned} \tag{4.64}$$

where $t_{phase}$ denotes the duration of the phase. As well, linear interpolation is done so that only the initial and final value of the mass in each phase is needed. This method will be used for the rest of variables which are defined as,

| | Climb | Cruise | Descent |
|---|---|---|---|
| $\gamma$ | $[3.0°,\ 0.0°]$ | $[0.0°,\ 0.0°]$ | $[0.0°,\ -3.0°]$ |
| $CL$ | $[0.5°,\ 0.5°]$ | $[0.7°,\ 0.7°]$ | $[0.5°,\ 0.5°]$ |
| *throttle* | $[0.95,\ 0.95]$ | $[0.85°,\ 0.85°]$ | $[0.03°,\ 0.03°]$ |
| $\mu$ | $[0.0°,\ 0.0°]$ | $[0.0°,\ 0.0°]$ | $[0.0°,\ 0.0°]$ |
| $t$ | $[300, 2000]$ | $[500, 14000]$ | $[300, 2000]$ |

Table 4.11: Initial guess using linear interpolation

In table 4.11 the first part of the vector denotes the initial value of the variable and the second term the final value of the variable for that phase. The rest mid-values are determined using linear interpolation. Additionally, the duration bounds for the climb and descent are normally sufficiently accurate. However, regarding the cruise, for routes longer than 4 hours the upper duration bound should be increased. Nevertheless, the number of points needed to compute that kind of route will exceed the allocated memory available (for a proper solution).

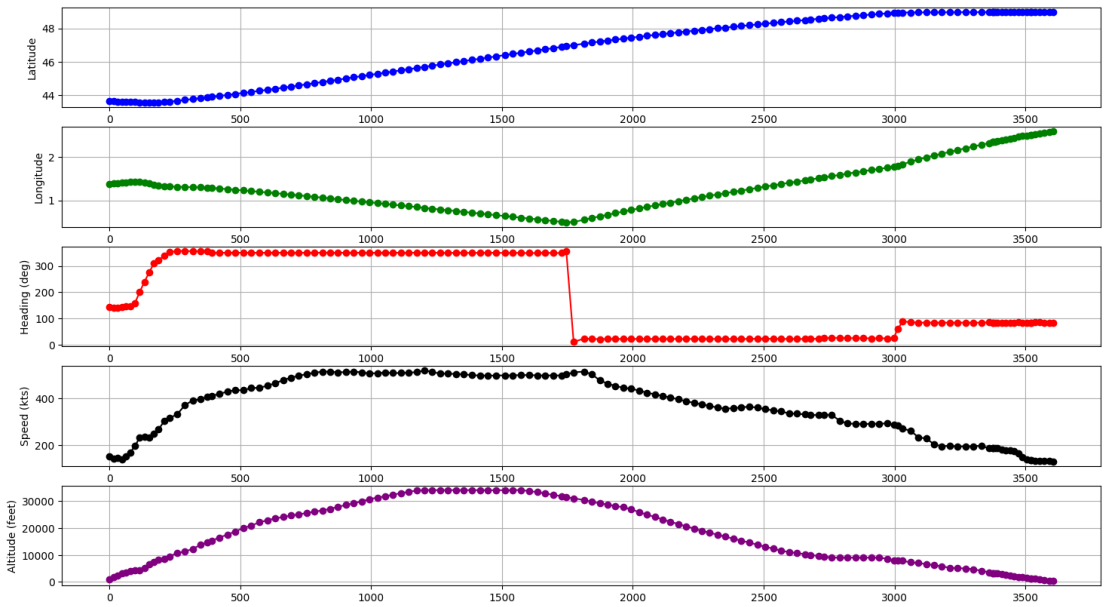


Figure 4.11: Toulouse-Paris Charles de Gaulle flight data from web scraping function

# 5 Results

## 5.1 Case Study 1: Analysis of Surrogate Model Performance

The reason behind the use of surrogate models is to develop a data-driven approach to build more realistic models and abandon the analytical formulations. In this study, the analytical models of propulsion and specific fuel consumption (SFC) are thought to be replaced using the information retrieved from the engine working at different conditions. Unfortunately, the information of the engine types that operates in the main commercial engines are confidential and not accessible. However, the analytical expressions defined in the BADA user manual have been used to simulate this engine data charts. In order to create the data chart, a statistical method for generating a quasi-random sampling distribution called *Latin Hypercube Sampling* from the *SMT* library have been introduced.

Both the propulsion and specific fuel consumption depends on the altitude, velocity and the throttle. The variables are bounded as,

$$\begin{aligned} h &\in [0m, 12000m] \\ mach &\in [0, 1] \\ \pi &\in [0, 1] \end{aligned} \tag{5.1}$$

Once the Latin Hypercube Sampling (LHS) has been utilized to define the data set for the propulsion and specific fuel consumption (SFC) systems, it is divided between test and training set as depicted in figure 5.1. This division enables the analysis of the performance of the surrogate models by evaluating how well it generalize the new data (test set).

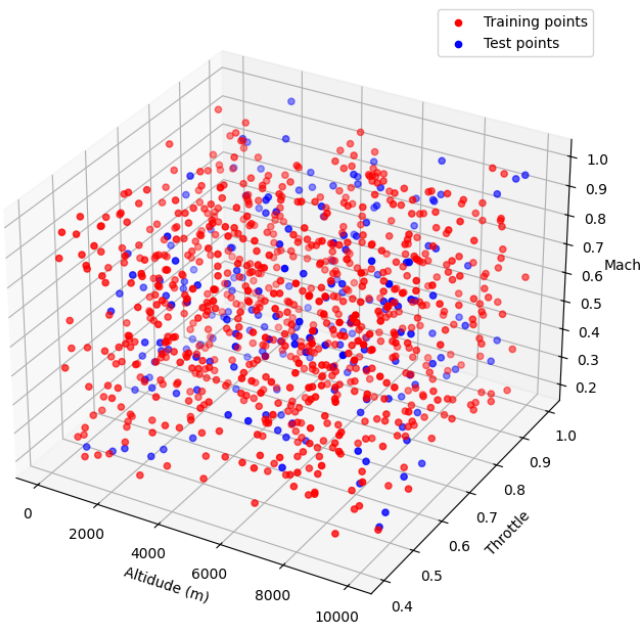


Figure 5.1: Test and training set for climb phase.

To evaluate how the surrogate models replicate the behaviour of the dataset used for training, two parameters are computed, the $R^2$ score and the root mean square error (RMSE). The $R^2$ score provides a measure of the proportion of the variance in the dependent variables that is predictable from the independent variables. $R^2$ scores close to 1 indicates that the model perfectly predicts the target variables. The RMSE measures the average squared difference between the actual target values and the predicted values. Lower values of RMSE indicate better model performance. In table 5.1 is presented the model evaluation. Given the medium size

database and the behaviour of the analytical models, Kringing method can replicate their evolution with a very high accuracy.

| Model | Phase | $R^2$ Score | RMSE |
|---|---|---|---|
| **Propulsion** | Climb | 0.999 | 0.0306 |
| | Cruise | 0.999 | 3.3357e-14 |
| | Descent | 0.999 | 0.0300 |
| **SFC** | Climb | 0.999 | 3.3357e-14 |
| | Cruise | 0.999 | 0.0306 |
| | Descent | 0.999 | 3.271e-11 |

Table 5.1: Evaluation of propulsion and SFC surrogate models in different phases

A route optimization problem has been set up in order to test the performance of the surrogate model by comparing its solution with the one using the BADA analytical expressions. It is not expected a reduction of the computational time when using the surrogate models because the analytical approaches are simple and do not need a big computational effort to be solved. The route to optimize is Madrid, Barajas (LEMD) - Paris, Charles de Gaulle (LFPG). The cost index is 0 so that the objective is to minimize the fuel consumption. The aircraft chosen to operate the flight is the Airbus A320 (Operation and Performance File in Appendix A).

As presented in figure 5.2a the main variables affected by this models which are the thrust, fuel flow rate and mass, present the same behaviour, except from a slight shift in the thrust for the climbing phase. Meanwhile the control variables represented by the lift coefficient, bank angle and throttle in figure 5.2b show a barely difference in the ascent phase. The reason behind it could lie on the fact that the accuracy of the thrust model during ascent shifts the local minimum of the optimization problem so that the CL decreases and the velocity increases, marginally, in the ascent phase. In fact, table 5.2 shows the flight time and fuel consumption where the difference is roughly 1 minute and 6 kilograms respectively.

Additionally, figure 5.3 displays the comparison of the SMT and analytical model. The state variables evolution is shown with only a slight difference in velocity and altitude, derived from the aforementioned higher lift coefficient for the analytical solution compared to the SMT solution .

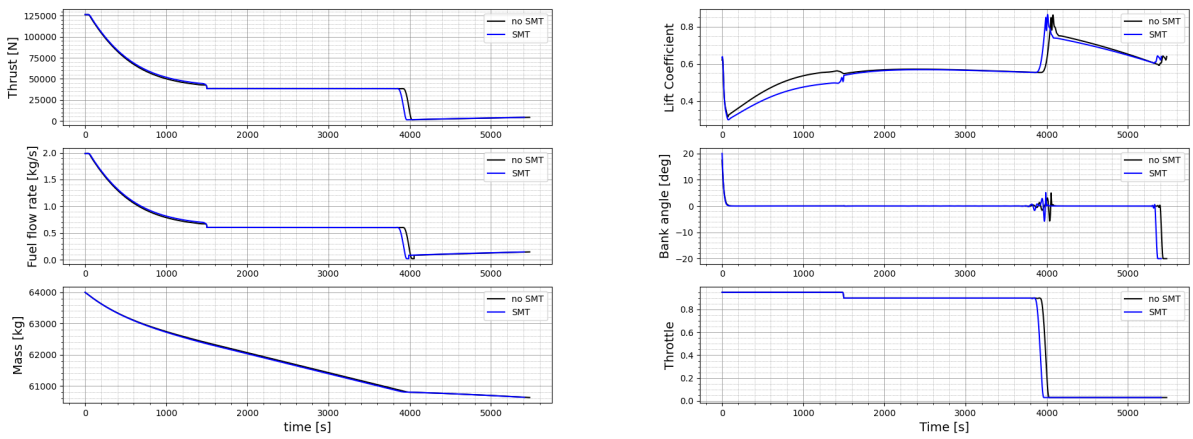


(a) Control variables

(b) States variables

Figure 5.2: Evolution of the solution for SMT and analytical model.

It is worth remarking that the objective of implementing surrogate models in this study is to have a data-driven approach and create more realistic and tailored models rather than creating faster ways of computing the

propulsive characteristics. This is the reason why it is only analyzed how well the surrogate models generalize the data using Kringing method whereas the computational time is not a key focus.

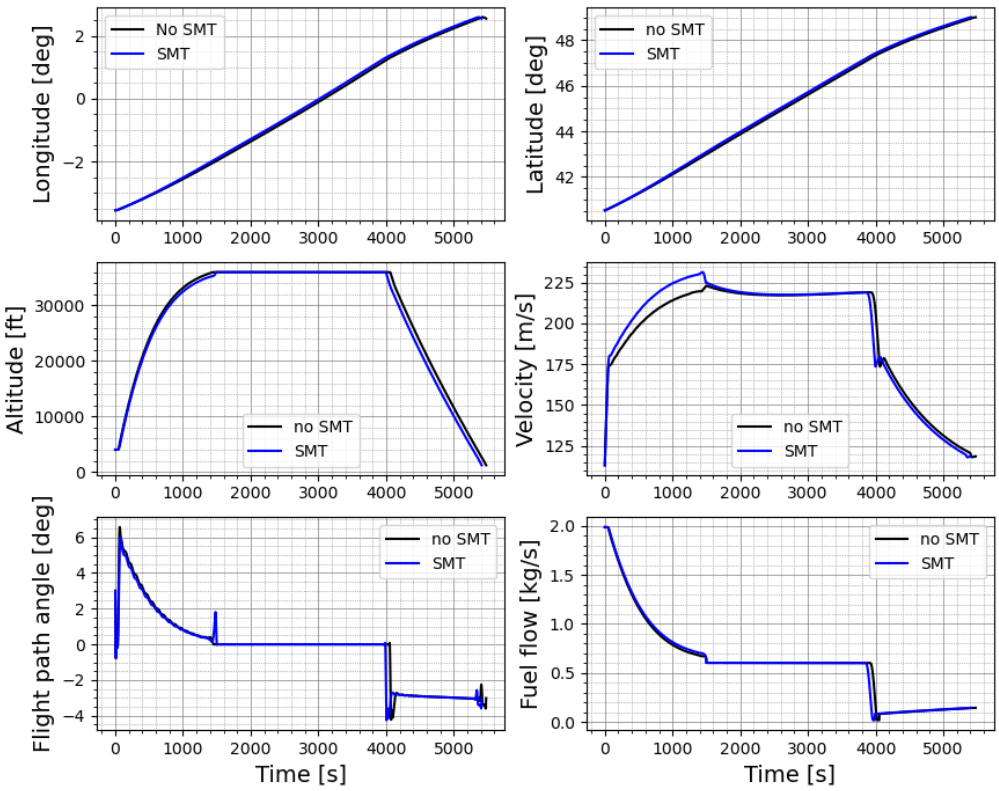


Figure 5.3: Comparison between SMT and analytical model

| | Time of flight | Fuel (kg) |
|---|---|---|
| **Madrid - Paris (SMT)** | 1h 30min 34s | 3377.92 |
| **Madrid - Paris (no SMT)** | 1h 31min 40s | 3384.53 |

Table 5.2: Time of flight and fuel consumption comparison between the analytical and surrogate model.

## 5.2 Case Study 2: Cost Index Influence. Pareto Front

The fundamental rational of the *Cost Index* (CI) concept is to achieve minimum operation trip cost by means of a trade-off between time related costs and fuel-related costs. Used appropriately, the CI feature of the flight management computer (FMC) can help airlines significantly reduce operating costs.

To have a wider scope of the impact of the cost index in the trajectory optimization problem, several optimizations will be undertaken with different values of CI from 0 to 100. The chosen route is Toulouse (LFBO) - Paris, Charles de Gaulle (LFPG) with the aircraft Airbus A320 (Operation and Performance File in Appendix A).

The results can be depicted in figure 5.4. The difference between taking into account the time-related costs and not, is remarkable. Between $CI = 0$ and $CI = 5$ the difference is 7.66 min and 86 kg of fuel, respectively. Additionally the the trend on the Pareto front follows a logarithmic trend. Figure 5.4b is a zoom in of the points

represented inside the square in figure 5.4a where some points which did not met the expected tendency have not been taken into account due to convergence issues.

The reader could think that the gap between the different CIs is minuscule. However the impact is greater if several flights per day are taken into account. Let's suppose the cost operations of two airlines, airline 1 with a cost index of 6 and airline 2 with a cost index of 40 and both airlines only have 1 aircraft. Generalizing the results in figure 5.4 the airline 1 is a 0.362% slower and burns a 0.126% of less fuel than airline 2. For the A320 family, the average time-related costs are 13 US$/min [3] whereas the actual cost of the kerosene is 1.26 US$/L (1.53 US$/kg) [23] (September 2024).

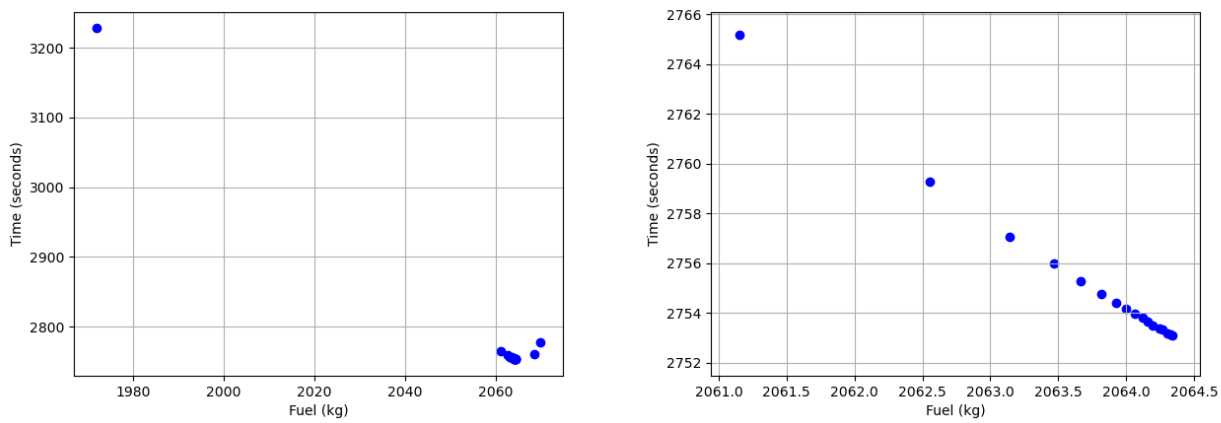


(a) Overall Pareto front

(b) Zoomed Pareto front

Figure 5.4: Pareto front for different Cost Index

Each airline does 5 flights per day. Now, let's assume that airline 1 does the 5 flights with a mean duration of 2 hours and a mean fuel consumption of 4800 kg. The competitor, airline 2, with a higher cost index will have the results presented in table 5.3. Airline 2 gives more importance to time than airline 1. As a consequence, the flight duration is shortened whereas the fuel consumption increases.

| | **1 day** | **1 year** |
|---|---|---|
| **ΔFlight duration** | −130.32 s | −13.2 h |
| **ΔTrip fuel** | 30.24 kg | 55 188 kg |

Table 5.3: Comparison of airline 1 over airline 2

Table 5.4 shows the time cost, fuel cost and the cost difference between airline 1 and airline 2 during the year. It is assumed that both airlines have the same time-related costs (13 US$/min). While airline 2 is saving 10 306 $ in time-related costs, it is increasing the fuel expense by 84 426 $. Thus, low-cost airlines will use lower cost indexes than higher-cost airlines.

| | **Time cost** | **Fuel cost** |
|---|---|---|
| **Airline 1** | 2 847 000 $ | 13 402 800 $ |
| **Airline 2** | 2 857 306 $ | 13 318 374 $ |
| **ΔCost** | −10 306 $ | 84 426 $ |

Table 5.4: Yearly cost difference between airlines 1 and 2

Finally, a route optimization between Madrid, Barajas (LEMD) - London, Heathrow (EGLL) has been set up

in order to compare the different optimal routes between $CI = 0$ and $CI = 100$, using the aircraft Airbus A320. As depicted in figure 5.5, the climb duration changes without changing the throttle position, and thus, the fuel consumption. In fact, the route with a higher CI takes a longer way to reach the cruising altitude aiming to get higher velocities in the ascent phase. Then, the duration of the cruise is greater for the route with $CI = 100$ finishing with an abrupt descent. To summarize, if time-related costs have a greater influence in optimization, the climb and descent phase are characterized by higher velocities, making the cruise phase longer while shortening the descent phase when prioritizing the time ($CI = 100$). On the other hand, the throttle is maintained at the same position during the flight in both configurations. Only, the aforementioned changes in climb and descent phases alter the duration of the flight, and thus, the fuel used.

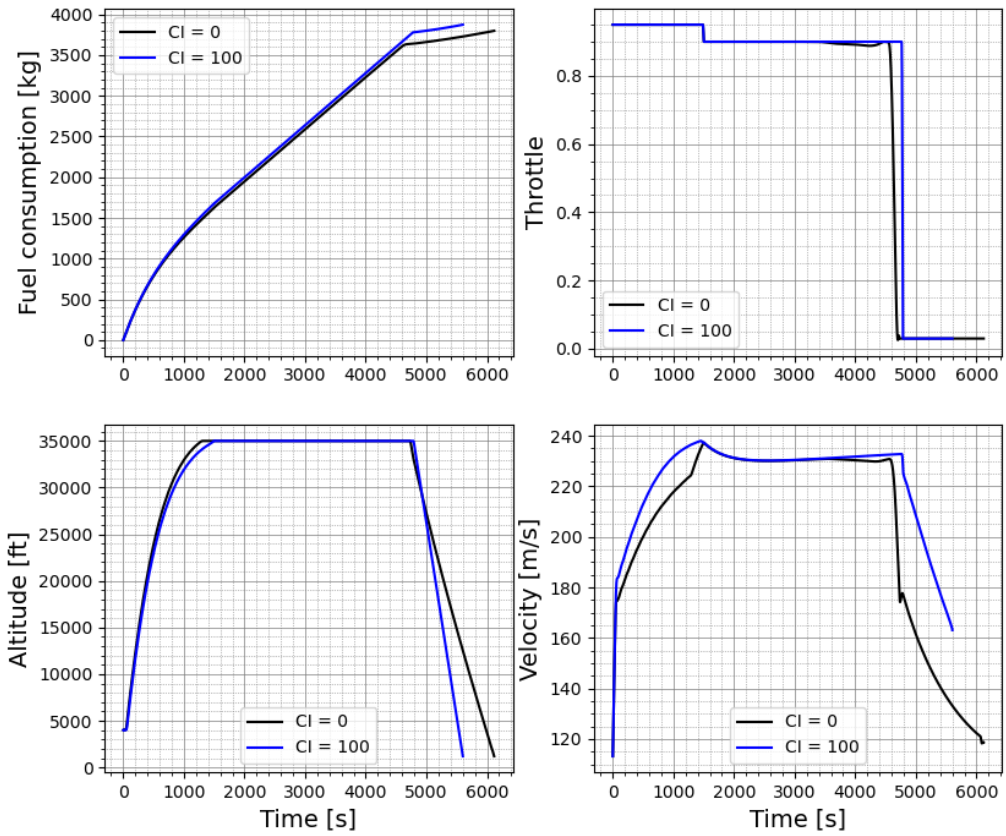


Figure 5.5: Evolution of different features for $CI = 0$ and $CI = 100$.

## 5.3 Case Study 3: Analysis of Wind Effects in Route Optimization

Aviation is deeply influenced by meteorology and its consequences. Rain, ice, snow, storms and winds are conditions to take into account when designing a route while minimizing costs. In this study, only the atmospheric wind is considered for the trajectory optimization. The main effect of the wind regarding fuel consumption and time is the jet streams presented in section 4.2.3.

To evaluate the wind effects, the following route has been set up: Madrid, Barajas (LEMD) - Reykjavik, Keflavik (BIKF) with the aircraft Airbus A320 (Operation and Performance File in Appendix A). The Cost Index is set to 0, so that the objective is to minimize the fuel used to complete the flight. The reason why this route was selected was to analyze a long route suitable for the A320 aircraft while experimenting the influence of the polar jet stream. The wind dataset retrieve from [16] corresponds to September 20th at 08.00h (UTC).

Figure 5.6a compares the results of the optimal path with wind (plotted in green, red and magenta for the different phases) and without wind (shown in black), utilizing a wind map for cruising altitude conditions. A clear deviation to western latitudes can be appreciated to avoid headwind from 45° to 52° in latitude and to tackle the strong lateral winds in higher latitudes due to the jet stream. Figure 5.6 shows the wind profile during the route. As expected, the prevailing winds are predominantly from the west (see u component) reaching velocities of up to 57 m/s (205 km/h). Hence, it is remarkable to point out the difference in time and, particularly, in fuel consumption between both trajectories. The introduction of wind effects increased the fuel utilized by 235 kg while shorten the duration of the flight by 4 minutes (table 5.6).

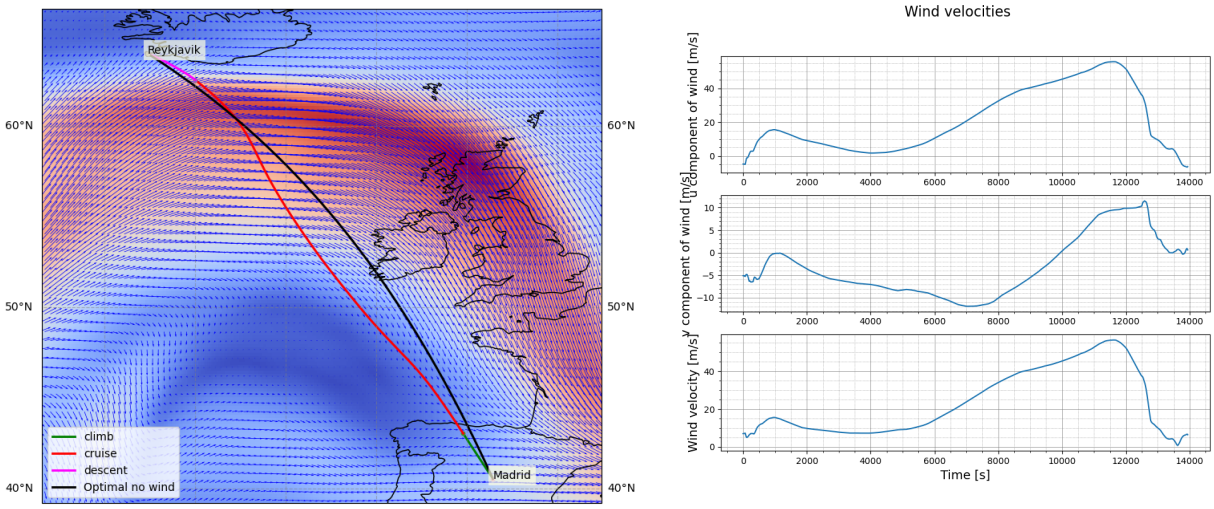


(a) Wind map route comparison

(b) Wind profile along the route

Figure 5.6: Analysis of the influence of wind

However, to proper evaluate the influence of the atmospheric winds, it is necessary to study long haul flights such as New York, John F. Kennedy International Airport (KJFK) - Madrid, Barajas (LEMD). Additionally, a new aircraft has to be used for this new route given that the A320 has not enough autonomy to complete it. Given the confidentiality and the difficult access to the OPF files and performance of the rest of aircrafts, the only available operation and performance file is the Airbus A306 [12] whose OPF file is specified in Appendix B. The aim of this route optimization is to evaluate how the polar jet stream can be used to reduce time and fuel consumption.

The results presented in table 5.6 show an important decrease in time taking 1 hour and 15 minutes less time and 4243 kg of less fuel to complete the route using the polar jet stream. If the assumption of 1.53 US$/kg for the fuel and 13 US$/min for the time cost is taken into account, 64 991 $ are saved for this flight. It is worth remarking that the jet stream, and particularly the polar jet stream, varies in latitude and strength depending on the season. Figure 5.7 shows the route paths in a wind map for the cruising altitude conditions (37000 ft) where the optimal path with wind (plotted in green, red and magenta for the different phases) and without wind (shown in black). The polar jet stream represents the reddish part of the map where the winds reach up to 250 km/h. The solution route with wind shows the tendency of the optimizer to replicate the pattern of the jet stream so that it can take advantage of the maximum amount of tailwind.

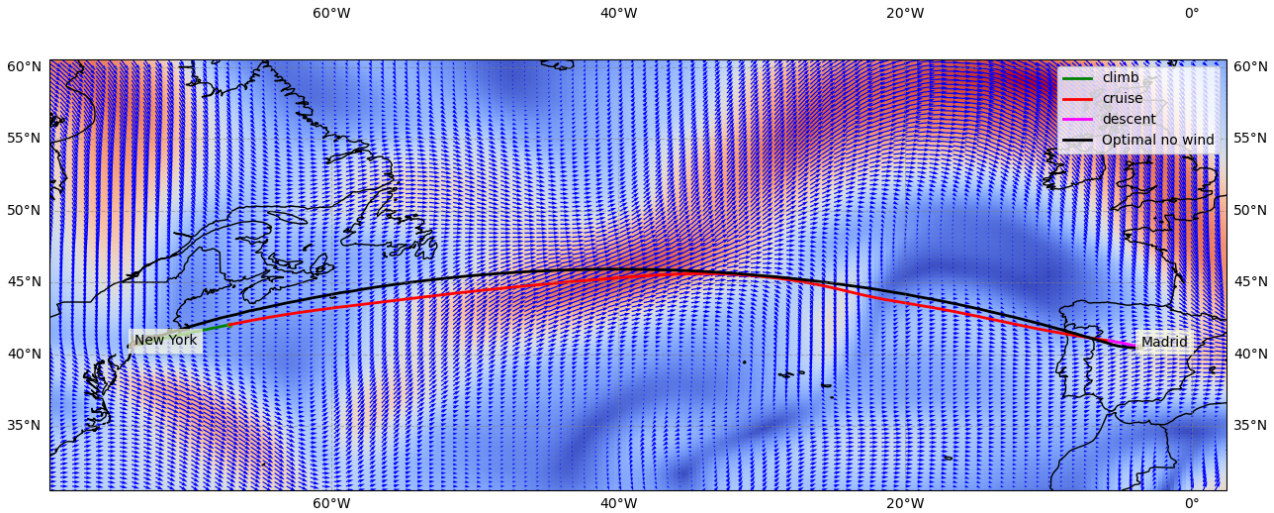


Figure 5.7: Wind map for a cruising altitude of h = 37000ft (11277m).

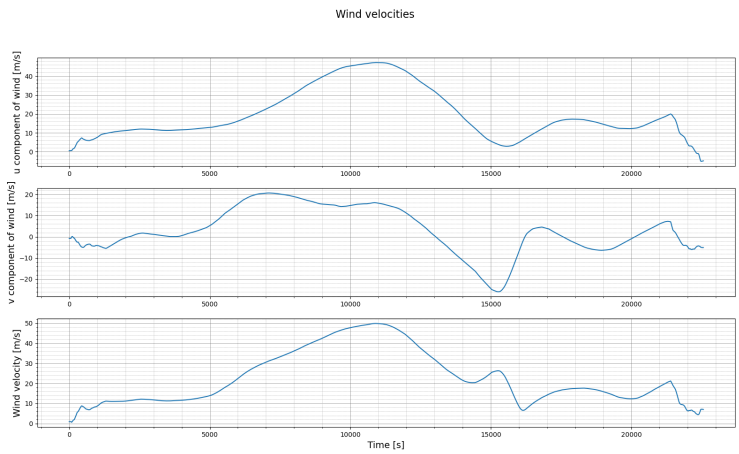


Figure 5.8: Wind profile for the route New York - Madrid

It is worth highlighting that the jet stream cannot help but hinder the optimization results for the inverse flight, from Madrid to New York, when flying in headwind. Now the objective will be to avoid the polar jet stream in an effort to avoid as much as possible the effects of headwinds. Given that the impact of the atmosphere behaviour is not negligible, the understanding of atmosphere and meteorology is a matter of paramount importance in aviation.

| | **Time of flight** | **Fuel (kg)** |
|---|---|---|
| **Madrid - Reykjavik** | 3h 48min | 8742.17 |
| **New York - Madrid** | 7h 31min | 32694.80 |

Table 5.5: Time of flight and fuel consumption without wind effects

| | **Time of flight** | **Fuel (kg)** | **ΔTime** | **ΔFuel (kg)** |
|---|---|---|---|---|
| **Madrid - Reykjavik** | 3h 52min | 8977.97 | 4.16min | 235 |
| **New York - Madrid** | 6h 15min | 28451.57 | 1h 15min | -4243.23 |

Table 5.6: Time of flight and fuel consumption with wind effects

# 6 Conclusions

The master thesis here presented, defines the construction of a solid and versatile optimization tool aiming to reduce the costs of operating an aircraft and its environmental impact. It has been developed inside the context of seeking for a way to connect the world using a more sustainable aviation. To be able to achieve this task, a complex problem has been built characterized by innovative approaches regarding the determination of the initial guess, the development of surrogate models and the introduction of atmospheric conditions. Thus, the tool has been able to meet the expectations established at the beginning of the internship. Now, an analysis of each objective will be undertaken highlighting what it has been achieved while evaluating the limitations.

- **O.1** The overall evaluation of the solver is positive. The convergence is ensured for a large variety of problems making it a robust tool which enables the user to explore different scenarios. The introduction of the cost index concept adds a more realistic approach due to the fact that it is currently used in the aeronautic industry and, particularly, within airlines. This feature allows the user to tailor the optimization with respect to the weight of time-related and fuel-related costs.

  However, there are some limitations in terms of convergence. There is a critical parameter called number of segments in the route settings (see Appendix C). This feature discretizes the trajectory. For longer routes, the number of segments should increase, particularly in the cruise phase. The reason behind it, is the apparition of dynamic effects such as the phugoid mode. In fact, if the the number of segments is such that the distance in time from one point to another is greater than the period of the dynamic mode, oscillations will appear which will hinder the convergence of the optimization.

  Hence, this modus operandi adds another limitation linked to memory allocation, restricting the longitude of the route that is desired to be optimize. It is not possible to increase the number of segments in the cruise phase endlessly. Depending on the computer, the memory destined to run a python script varies.

- **O.2** and **O.3** The generation of an automatic initial guess has been one of the main concerns in this thesis. The function in charge of retrieving the information from Flight Aware [1] works for every scenario that has been tested. The possibility of retrieving real flight data and introduce it in the optimizer as initial guess has enabled the tool to rocket to a more user-friendly and robust optimizer. This feature makes easier to explore different routes very quickly. However, it presents some restrictions. As the data retrieved comes from a website which can change the format or the way the data is accessed anytime, it requires maintenance and updates. As well, it only works with the browsers *Mozilla Firefox* [21] and *Google Chrome* [15].

- **O.4** The variety of routes that has been explored along this master thesis shows how versatile the tool is. From Reykjavik to New York a wide range of scenarios with different restrictions can be set and analyzed. However there is a limitation regarding the heading angle. The optimizer does not manage well the discontinuities from 180° to −180°. So, routes which imply going south will face convergence difficulties because of the heading discontinuity. Nevertheless it is possible to change the bounds for the heading angle from 0° to 360° and run routes heading south. Further on, when presenting future work, an approach to tackle this problematic will be exposed. Moreover, if including the wind in the optimization process, the user must be aware that the wind model developed does not include the whole globe (a certain subregion has been selected to decrease the amount of unused data) and only corresponds to a certain date. If a new updated model is desired to be created, the most recent available data [16] is from 5 days ago.

- **O.5** Another key challenge faced in this master study has been the generation of surrogate models. The definition of two different methods to create the surrogate models (Kringing and Neural Network) comes from the fact that two distinct datasets are handled. Propulsion and fuel consumption datasets are medium sized and presents a smooth evolution able to be replicated by the Kringing method. For this reason, table 5.1 presents such high accuracies. Conversely, the model concerning the atmospheric wind is harder to replicate (see figure 4.9). The wind behaviour is chaotic with sudden changes in longitude, latitude and

height, which hinder the creation of a surrogate model. Although a precision of 97% is reached, the abrupt changes of wind are not accurately followed by the model. Hence, there has not been a deep sensitivity study in the selection of the hyperparameters for the Neural Network such as batch size, number of layers or number of nodes per layer. However it is a sufficiently close approach to the objective of this master thesis. The influence and introduction of wind have been successfully evaluated.

# 7 Future Work

Besides the fulfillment of all the objectives and the successful results presented, there is room for improvement. Firstly, it is imperative to solve the heading angle discontinuity, by working with sinusoidal functions instead of angles. The sinusoidal functions do not present discontinuities between 0° and 360°. However it will add another equation to the equations of motion, and thus, increasing the complexity of the problem.

Another key challenge that will have to be tackled in the future is the introduction of phases such as the take off, approach and landing. Although those phases represents a short segment of the total route and will not affect very much the objective function, they are important phases to take into account for commercial aircraft trajectories. Furthermore, the introduction of airways will increment the level of realism of the optimization solution.

Airways are predefined routes in the sky that aircrafts follow during flight, functioning as the aerial equivalent of highways for planes. The existence of airways comes from the fact that the air traffic density is very high and there is a need to organize and control all the flights. By implementing this feature, the solution will be more realistic and applicable to real cases in the aviation industry.

Additionally, the tool assumes a stationary wind behavior, meaning that wind intensity and direction remain constant throughout the entire flight. Incorporating time-varying wind models would significantly improve the solver's resemblance to reality. Therefore, for future route plannings, the integration of available meteorological forecasts could help to optimize path selection and better organize flight routes.

Finally, the introduction of real engine data will help to create more realistic data-driven models in order to simulate accurately the powerplant behaviour.

# Appendix A: A320 OPF File

| Category | Details |
|---|---|
| **File Name** | A320.OPF |
| **Aircraft Type** | Airbus A320-212 with CFM56 engines, 2 engines |
| **Mass (in tons)** | Reference: 64.00 t<br>Minimum: 39.00 t<br>Maximum: 77.00 t<br>Max Payload: 21.50<br>Mass Gradient: 0.28 |
| **Flight Envelope** | VMO (KCAS): 350.00<br>MMO: 0.82<br>Maximum Altitude: 39,000 ft<br>Temperature Gradient: -130.00 |
| **Aerodynamics** | Wing Area: 122.60 m²<br>Buffet Coefficients (SIM): Clbo (M=0): 0.000<br>Configuration Characteristics:<br>Clean: Vstall: 145 KCAS, CD0: 0.024, CD2: 0.0375<br>Flap15 (IC): Vstall: 120 KCAS, CD0: 0.0242, CD2: 0.0469<br>Flap15 (TO): Vstall: 114 KCAS, CD0: 0.0393, CD2: 0.0396<br>Flap15 (AP): Vstall: 107 KCAS, CD0: 0.0456, CD2: 0.0381<br>Flap30 (LD): Vstall: 101 KCAS, CD0: 0.0838, CD2: 0.0371<br>Spoiler Coefficients (EXT): 0.000<br>Gear (DOWN): CD0: 0.0312 |
| **Engine Thrust** | Max Climb Thrust Coefficients (SIM): 13605 kN |
| **Fuel Consumption** | Thrust Specific Fuel Consumption Coefficients: 0.940<br>Descent Fuel Flow Coefficients: 88.90, 81926 |
| **Ground Specifications** | Take-off Length: 2190 m<br>Landing Length: 1440 m<br>Wingspan: 34.1 m<br>Aircraft Length: 37.57 m |

# Appendix B: A306 OPF File

| Category | Details |
|---|---|
| **File Name** | A306.OPF |
| **Aircraft Type** | Airbus A300-B4-622 with PW4158 engines, 2 engines, Jet H |
| **Mass (in tons)** | Reference: 140.00 t<br>Minimum: 87.00 t<br>Maximum: 171.70 t<br>Max Payload: 39.00 t<br>Mass Gradient: 0.141 |
| **Flight Envelope** | VMO (KCAS): 335.00<br>MMO: 0.82<br>Maximum Altitude: 41,000 ft<br>Temperature Gradient: -67.00 |
| **Aerodynamics** | Wing Area: 260.00 m²<br>Buffet Coefficients (SIM): Clbo (M=0): 1.530<br>Configuration Characteristics:<br>Clean: Vstall: 151 KCAS, CD0: 0.0190, CD2: 0.053<br>Flap15 (IC): Vstall: 117 KCAS, CD0: 0.0331, CD2: 0.0454<br>Flap15 (TO): Vstall: 117 KCAS, CD0: 0.0331, CD2: 0.0454<br>Flap15 (AP): Vstall: 109 KCAS, CD0: 0.0380, CD2: 0.0449<br>Flap30 (LD): Vstall: 97 KCAS, CD0: 0.0789, CD2: 0.0448<br>Spoiler Coefficients (EXT): 0.000<br>Gear (DOWN): CD0: 0.0225 |
| **Engine Thrust** | Max Climb Thrust Coefficients (SIM): 3040 kN<br>Descend Coefficients: low: 0.073, high: 0.206<br>Desc Level: 80,000 ft<br>Desc App: 1.20<br>Desc LD: 3.60<br>Desc CAS: 280 KCAS<br>Desc Mach: 0.79 |
| **Fuel Consumption** | Thrust Specific Fuel Consumption Coefficients: 0.881<br>Descent Fuel Flow Coefficients: 26.805, 457,000<br>Cruise Correction: 1.038 |
| **Ground Specifications** | Take-off Length: 2362 m<br>Landing Length: 1555 m<br>Wingspan: 44.84 m<br>Aircraft Length: 54.08 m |

# Appendix C: Set up a route

| Input Parameter | Description |
|---|---|
| `route_settings['aircraft']` | Aircraft type for the trajectory optimization (e.g., 'A320'). |
| `route_settings['departure']` | Dictionary containing information about the departure airport:<br>- `airport`: ICAO code (e.g., 'LEMD')<br>- `latitude`: Latitude of the airport<br>- `longitude`: Longitude of the airport<br>- `rwy_course`: Runway course in degrees<br>- `altitude`: Altitude in feet |
| `route_settings['arrival']` | Dictionary containing information about the arrival airport:<br>- `airport`: ICAO code (e.g., 'LFPG')<br>- `latitude`: Latitude of the airport<br>- `longitude`: Longitude of the airport<br>- `rwy_course`: Runway course in degrees<br>- `altitude`: Altitude in feet |
| `route_settings['browser']` | The browser used to extract data (e.g., 'firefox'). |
| `route_settings ['Performance_model']` | Performance model file (e.g., BADA file). |
| `route_settings ['Propulsion_Surrogate_model']` | Flag indicating whether a propulsion surrogate model is used (True/False). |
| `configurations['climb', 'cruise', 'descent']` | Flight phase configurations:<br>- `num_segments`: Number of segments in each phase<br>- `order`: Polynomial order for each phase |
| **Output** | Trajectory setup ready to be optimized (e.g., `traj_prob`). |

Table 7.3: Inputs and Outputs of the Aircraft Trajectory Optimization Function

# References

[1] Flightaware. https://www.flightaware.com/, 2024.

[2] Felipe Miguel Aparicio Acosta. Radial basis function and related models: An overview. *Signal Processing*, 45(1):37–58, 1995.

[3] Airbus. *Getting to Grips with the Cost Index*, issue ii edition, May 1998. Published by Airbus.

[4] J.D. Anderson. *Introduction to flight*. McGraw Hill, 2000.

[5] John T. Betts. Survey of numerical methods for trajectory optimization. *Journal of Guidance, Control, and Dynamics*, 21(2):193–207, 1998.

[6] Mohamed Amine Bouhlel, John T. Hwang, Nathalie Bartoli, Rémi Lafage, Joseph Morlier, and Joaquim R. R. A. Martins. A python surrogate modeling framework with derivatives. *Advances in Engineering Software*, page 102662, 2019.

[7] Arthur E. Bryson, Y.-C. Ho, and George M. Siouris. Applied optimal control: Optimization, estimation, and control. *IEEE Transactions on Systems, Man, and Cybernetics*, 9:366–367, Jul 1979.

[8] Visual Capitalist. Visualizing well-known airlines by fleets. https://www.visualcapitalist.com/visualizing-well-known-airlines-by-fleets/, 2024. Accessed: September 4, 2024.

[9] Bruce A. Conway. A survey of methods available for the numerical optimization of continuous dynamic systems. *Journal of Optimization Theory and Applications*, 152(2):271–306, Feb 2012.

[10] SMT Documentation. Kriging model — surrogate modeling toolbox. https://smt.readthedocs.io/en/latest/_src_docs/surrogate_models/gpr/krg.html, 2024. Accessed: 2024-09-10.

[11] G. Dreyfus. *Neural Networks: Methodology and Applications*. Springer-Verlag Berlin Heidelberg, 1 edition, 2005.

[12] EUROCONTROL Experimental Centre. *Base of Aircraft Data (BADA) User Manual*, June 2023. Version 4.2.

[13] Robert Falck, Justin S. Gray, Kaushik Ponnapalli, and Ted Wright. dymos: A python package for optimal control of multidisciplinary systems. *Journal of Open Source Software*, 6(59):2809, 2021.

[14] David Morente González. Hybrid multi-objective trajectory optimzation of low-thrust space mission design. MS Thesis, Universidad Carlos III de Madrid, 2019.

[15] Google. Google chrome browser. https://www.google.com/intl/es_es/chrome/, 2024. Accessed: 2024-10-03.

[16] H. Hersbach, B. Bell, P. Berrisford, G. Biavati, A. Horányi, J. Muñoz Sabater, J. Nicolas, C. Peubey, R. Radu, I. Rozum, D. Schepers, A. Simmons, C. Soci, D. Dee, and J-N. Thépaut. Era5 hourly data on pressure levels from 1940 to present, 2023. Copernicus Climate Change Service (C3S) Climate Data Store (CDS), DOI: 10.24381/cds.bd0915c6 (Accessed on 16-09-2024).

[17] David G. Hull. *Fundamentals of Airplane Flight Mechanics*. Springer, 2007.

[18] Jack P.C. Kleijnen. Kriging: Methods and applications. 2017.

[19] R. Marler and Jasbir Arora. Survey of multi-objective optimization methods for engineering. *Structural and Multidisciplinary Optimization*, 26:369–395, Apr 2004.

[20] Melanie Mitchell. *An Introduction to Genetic Algorithms*. MIT Press, Cambridge, MA, USA, 1998.

[21] Mozilla. Firefox browser. https://www.mozilla.org/es-ES/firefox/new/, 2024.

[22] National Oceanic and Atmospheric Administration (NOAA). Jetstream: Jet stream - global. https://www.noaa.gov/jetstream/global/jet-stream, 2023. Accessed: 2024-09-18.

[23] New York State Energy Research and Development Authority. Monthly average kerosene prices. https://www.nyserda.ny.gov/Energy-Prices/Kerosene/Average-Kerosene-Prices, 2024. Accessed: 2024-10-01.

[24] William S. Noble. What is a support vector machine? *Nature Biotechnology*, 24:1565–1567, 2006.

[25] Eva Ostertagová. Modelling using polynomial regression. *Procedia Engineering*, 48:500–506, 2012. Modelling of Mechanical and Mechatronics Systems.

[26] Aakash Parmar, Rakesh Katariya, and Vatsal Patel. A review on random forest: An ensemble classifier. In Jude Hemanth, Xavier Fernando, Pavel Lafata, and Zubair Baig, editors, *International Conference on Intelligent Data Communication Technologies and Internet of Things (ICICI) 2018*, pages 758–763, Cham, 2019. Springer International Publishing.

[27] Adam Paszke, Sam Gross, Francisco Massa, Adam Lerer, James Bradbury, Gregory Chanan, Trevor Killeen, Zeming Lin, Natalia Gimelshein, Luca Antiga, Alban Desmaison, Andreas Kopf, Edward Yang, Zachary DeVito, Martín Raison, Alykhan Tejani, Sasank Chilamkurthy, Benoit Steiner, Lu Fang, Junjie Bai, and Soumith Chintala. Pytorch: An imperative style, high-performance deep learning library, 2019.

[28] Riccardo Poli, James Kennedy, and Tim Blackwell. Particle swarm optimization: An overview. *Swarm Intelligence*, 1, Oct 2007.

[29] L. S. Pontryagin. *Mathematical theory of optimization processes*. 1962.

[30] Anil V. Rao. A survey of numerical methods for optimal control. *Advances in the Astronautical Sciences*, 135(1):497–528, 2009.

[31] Damián Rivas Rivas. *Mecánica de Vuelo*. Escuela Técnica Superior de Ingeniería, 2016.

[32] P. Saves, R. Lafage, N. Bartoli, Y. Diouane, J. Bussemaker, T. Lefebvre, J. T. Hwang, J. Morlier, and J. R. R. A. Martins. SMT 2.0: A surrogate modeling toolbox with a focus on hierarchical and mixed variables gaussian processes. *Advances in Engineering Sofware*, 188:103571, 2024.

[33] Vivek Yadav. Direct collocation. https://mec560sbu.github.io/2016/09/30/direct_collocation/, 2016. Accessed: 2024-09-10.

[34] Jinming Zou, Yi Han, and Sung-Sau So. *Overview of Artificial Neural Networks*, pages 14–22. Humana Press, Totowa, NJ, 2009.